Ecology and Evolution of Bacteria across Host Scales

by

Killian Campbell

A dissertation accepted and approved in partial fulfillment of the

requirements for the degree of

Doctor of Philosophy

in Biology

Dissertation Committee:

Brendan Bohannan, Chair

Matthew Barber, Advisor

Andrew Kern, Core Member

Melanie Spero, Core Member

Michael Harms, Institutional Representative

University of Oregon

Fall 2025

DISSERTATION ABSTRACT

Killian Campbell

Doctor of Philosophy in Biology

Title: Ecology and Evolution of Bacteria Across Host Scales

Bacteria are an extremely diverse domain of life, representing a breathtaking array of form and function. Many bacteria establish intimate relationships with host organisms where they exist as commensal members of the host's microbiome, shaping fundamental components of the host's physiology, health and development. Despite the sizeable influence of microbiomes on host development, it is unknown how microbiomes assemble on host organisms. It has been proposed that neutral ecological processes may affect the assembly of microbiomes, but it is unclear the degree to which that is true. Conversely, bacteria can maintain pathogenic relationships with hosts where they exert antagonistic effects on host organisms when they establish infections of those host organisms. To do this, pathogenic bacteria must circumvent the pressures they encounter in the host environment to successfully infect a host. In this thesis, I address gaps in the literature for each of these areas of research. Firstly, to better understand the forces that govern microbiome assembly, I investigated the relative importance of neutral ecological processes on the tissue-specific assembly of microbiomes across a panel of diverse animal hosts. Importantly, I discovered a potentially broad scale pattern of neutral ecological processes playing an outsized role in the assembly of microbiomes in external tissues compared to internal tissues. Secondly, to understand how pathogens evolve to resist host-encoded pressures, I focused on the human pathogen *Staphylococcus aureus (S. aureus),* and how it evolves resistance to polyamines, a class of host-encoded molecules that are uniquely toxic to *S. aureus.* In my investigations of *S. aureus,* I discovered that the evolution of resistance to

polyamines occurred primarily through mutations that altered potassium transport machinery, and that these mutations conferred collateral resistance to other known antimicrobials. Overall, this work contributes significant knowledge to the microbiome and *S. aureus* literature.

This dissertation includes previously published and coauthored material.

ACKNOWLEDGMENTS

First and foremost, I wish to acknowledge my husband, Benjamin Kerner for his unwavering love and support of me during my time in graduate school. He has been my biggest supporter, advocate, and friend during this entire process. There is no world in which I complete this degree without his love and support, and for that I am profoundly thankful.

I would also like to thank my family: To my parents, who imparted a sense of curiosity and irreverence, and allowed me to be the weird, intellectual, offbeat kid that I was. I would not have become a scientist if it weren't for the intricate ways that you exposed the world to me. To my extended family: Chris and Sue, thank you for being wonderful supporters of my career, and allowing me to move your son to random parts of the country every few years. This support is more important than you know.

I would like to thank my advisor, Dr. Matthew Barber. Matt graciously made a case for me to join the UO Biology Graduate Program as a transfer student, and for this I will always be thankful. Matt's mentorship and ability to allow me to explore my interests were invaluable to my development as an independent scientist. Even when I doubted the importance of my own work, Matt provided me with the support and space needed to get through the hard times.

I would also like to thank my ("unofficially official") second advisor Dr. Brendan Bohannan. Brendan, I am so thankful for all the conversations we had during graduate school, both scientific and otherwise. I felt a very special sense of inclusion with your group, and I enjoyed learning to think more "ecologically" and "philosophically", while spending time in your group. I especially admire your capacity to lead with curiosity, not judgement, no matter the situation at hand. I always felt like your lab was a second home. I also need to thank Dr. Karen

Adair, who skillfully and patiently taught me how to use R and analyze microbiome data. I frequently found myself impressed by your ability to ask insightful questions.

To the rest of the Barber lab: Dr. Caitlin Kowalski, you are in many ways the other advisor I was fortunate enough to work with during my PhD. I would not have made it through this degree without your excellent mentorship, scientific acumen, and kind, yet critical feedback. You pushed me to be excellent and set a great example for what a successful scientist looks like. You also brought an inspiring energy to the group that made the hard days so much better. To the rest of the Barber Lab: Thank you Titas, Kendal, Dante', Sylvia, Mara and Grace for being such wonderful colleagues. Coming to work every day was truly made better because I had the privilege of sharing it with you all.

I also must thank the mentors that I was fortunate enough to have learned from before: Andrea Castillo, Benjamin Flanagan, Tera Levin, and Harmit Malik, each of you changed my life in ways I will never forget.

Lastly, thank you to my best friend, Dr. Danica Schmidtke. I truly don't think I would have made it through this degree without your friendship. I am not sure many people get to experience so many monumental milestones in tandem with their best friend, and for that I think we are profoundly lucky.

DEDICATION

I dedicate this thesis, to my grandparents, Phil and Olive Guinand, who helped show me the world.

TABLE OF CONTENTS

LIST OF FIGURES

LIST OF TABLES

Table Page

CHAPTER I.

INTRODUCTION

Microorganisms are everywhere, inhabiting virtually every environment on earth (1). Bacteria are one such domain of microorganisms that demonstrate a breathtaking amount of diversity in both physical form and physiological function. Due to their ubiquitous nature and vast diversity, animal host organisms exhibit a variety of interactions with bacteria, ranging from pathogenic to beneficial. Despite the pervasiveness of these interactions, the various factors that determine outcomes of host colonization by bacteria are poorly understand. One reason for this gap in understanding is that there are multiple phases of interaction between hosts and bacteria, and each of these phases is governed by different forces. For example, to establish a relationship with a host organism, a bacterium must first disperse and successfully colonize a host. Colonization may be affected by both deterministic and stochastic factors, although the relative importance of each factor is hotly debated (2). Following colonization, the bacterium may persist on the host as a commensal member of the microbiota or, if pathogenic, establish an infection. Effectively understanding each of these phases requires studying bacteria at different scales with diverse methods. In this work, I studied host-bacteria interactions across different scales and phases of interaction, investigating the forces that shape both host colonization by microbes, and the forces that shape survival during an infection of the host.

In Chapter II, I investigated the role of neutral ecological processes on the tissue specific assembly of animal microbiomes. While animal-associated microbiomes are widely studied, the various factors that contribute to the assembly of these microbiomes remains elusive. Previous work has identified that neutral ecological processes play a role in the assembly of microbiomes

(2). However, these examples are relatively isolated to specific host organisms and single anatomical sites on the animal hosts studied (3, 4). Furthermore, no work to date has taken a comparative approach to studying the role of neutral processes in microbiome assembly across a panel of animal hosts. To do this, I identified previously published microbiome sequencing datasets for a panel of diverse animal hosts. With this data I fit ecological models to 16s rRNA sequencing data to explain the observed levels of diversity in the microbiomes of different animal hosts. Critically, I determined if neutral processes were more important to microbiome assembly in external (skin or scale) or internal (gut) tissues. Previously, neutral processes had been reported as an important driver of microbiome assembly. However, it is unknown which anatomical sites that this may be most important for, and if this is rare example or widespread trend. This chapter is published in the journal Microbiology Spectrum (https://doi.org/10.1128/spectrum.02223-25) and was coauthored with Dr. Karen Adair and Dr. Brendan Bohannan.

In Chapter III, I focus on a single species of human pathogen, *Staphylococcus aureus,* and how it evolves resistance to a class of host-encoded molecules known as polyamines. Polyamines are present in diverse organisms across the tree of life (5). They are ancient and believed to have been present in the last universal common ancestor. As a result, many species of bacteria produce or acquire polyamines to support their normal physiology. Despite this, *S. aureus* lacks the capability to synthesize polyamines and is killed upon exposure to physiological concentrations of them. Furthermore, *S. aureus* is exposed to polyamines in the host environment, particularly during skin and soft tissue infections (SSTI) of the human host (6). This presents a conundrum: how does *S. aureus* circumvent this pressure in the host environment? To answer this question, I used an experimental evolution approach to study how

resistance to polyamines evolves in the laboratory in three different strain backgrounds of *S. aureus.* This work revealed that evolution occurs differently, dependent on genomic context of the strain, and that evolving polyamine resistance poses major consequences for collateral phenotypes such as antibiotic resistance. This work was co-authored with Dr. Caitlin Kowalksi, Dr. Kristin Kohler, Mara Kebret, and Dr. Matthew Barber. This work has been published in mSphere (https://doi.org/10.1128/msphere.00613-24).

In Chapter IV I speculate on the potential mechanistic bases of polyamine resistance and propose future work to follow up on the discoveries generated in chapter III. I specifically focus on mutations that I identified in the Ktr potassium transport complex and speculate on how mutations in this complex may alter Ktr function and global gene expression profiles in *S. aureus.* This chapter does not contain any published work, and the data within it was generated by me. The ideas for the experiments originated as a series of conversations between Dr. Matthew Barber and me.

Together, these chapters address a key knowledge gap at the intersection of microbiology, ecology and evolution. Chapter II contributes significantly to the microbiome literature by providing novel evidence for tissue-specific roles of neutral ecological processes in microbiome assembly. Chapter III contributes significantly to the *S. aureus* literature by documenting the first connection between potassium transport and polyamine resistance in *S. aureus*.

References

1. Lozupone, C.A. and Knight, R., 2007. Global patterns in bacterial diversity. *Proceedings of the National Academy of Sciences*, *104*(27), pp.11436-11440.

2. Heys, C., Cheaib, B., Busetti, A., Kazlauskaite, R., Maier, L., Sloan, W.T., Ijaz, U.Z., Kaufmann, J., McGinnity, P. and Llewellyn, M.S., 2020. Neutral processes dominate microbial community assembly in Atlantic salmon, Salmo salar. *Applied and Environmental Microbiology*, *86*(8), pp.e02283-19.

3. Burns, A. R., Stephens, W. Z., Stagaman, K., Wong, S., Rawls, J. F., Guillemin, K., & Bohannan, B. J. 2016. Contribution of neutral processes to the assembly of gut microbial communities in the zebrafish over host development. *The ISME journal*, *10*(3), 655–664.

4. Venkataraman, A., Bassis, C. M., Beck, J. M., Young, V. B., Curtis, J. L., Huffnagle, G. B., & Schmidt, T. M. 2015. Application of a neutral community model to assess structuring of the human lung microbiome. *mBio*, *6*(1), e02284-14. https://doi.org/10.1128/mBio.02284-14

5. Michael, A.J., 2016. Polyamines in eukaryotes, bacteria, and archaea. *Journal of Biological Chemistry*, *291*(29), pp.14896-14903.

6. Thurlow LR, Joshi GS, Clark JR, Spontak JS, Neely CJ, Maile R, Richardson AR. 2013. Functional Modularity of the Arginine Catabolic Mobile Element Contributes to the Success of USA300 Methicillin-Resistant Staphylococcus aureus. Cell Host Microbe 13:100–107.

CHAPTER II
SKIN/SCALE MICROBIOMES ARE MORE NEUTRAL THAN GUT MICROBIOMES ACROSS MULTIPLE ANIMAL HOSTS

From: From Campbell, Adair, and Bohannan. 2025. Assembly of skin microbiomes is more neutral than gut microbiomes in multiple animal species. Microbiology Spectrum 10.1128/spectrum.02223-25

This chapter is accepted for publication in Microbiology Spectrum. Karen L. Adair and Brendan Bohannan are co-authors on this manuscript. This project originated as a rotation project in the Bohannan lab during the summer of 2020. This project was fully computational. I conducted the analyses for the project and took the lead on writing the manuscript. Karen L. Adair provided valuable intellectual guidance on the direction of the project and helped revise the manuscript. Brendan Bohannan also provided intellectual guidance for the project, edited the manuscript, and secured funding to conduct the work.

Introduction

Animal microbiomes are complex assemblages of microorganisms that influence a wide variety of host phenotypes. Despite their importance we lack a thorough understanding of the processes that guide the formation of microbiomes (i.e. microbiome assembly). Understanding how microbiomes assemble is essential to managing microbiomes for host health, conservation, and other goals. Most animals are colonized by communities of microorganisms that influence their development, health, and fitness (1,2). In healthy individuals, these host-associated microbial communities, or microbiomes, are predominantly found in the gastrointestinal tract,

respiratory system, and external tissues (e.g. skin or scales; refs). It is clear that microbiome composition is strongly influenced by body site (3-6) but the ecological processes that underlie this variation remain unclear. Two main types of processes contribute to the assembly of a microbiome over relatively short time scales. Selective processes are the result of fitness differences among members of a community. Examples of selective factors include variation in oxygen tolerance, ability to grow on specific carbon sources, and competitive or mutualistic interactions (1,2). In contrast, neutral processes are selectively neutral with respect to fitness, and instead are the result of purely stochastic events. Examples of neutral processes include ecological drift (random birth and death of individuals in a community) and passive dispersal of individuals (for example, random sampling of individual colonists from a source pool) (7,8). Understanding the relative roles of selective and neutral processes in microbiome assembly is essential to managing microbiomes for host health, conservation, and other goals (8).

Here we investigate whether the contributions of neutral processes differ between external (e.g. skin or scales) and internal (i.e. gastrointestinal tract) host tissues, and whether these patterns are consistent across host taxa.

Methods

Read Acquisition and Processing

I identified 16 published datasets that used 16S rRNA gene amplicon sequencing to characterize both the external and gut microbiomes of at least 20 individuals in a set of diverse animal hosts, including humans (TABLE 2.1). For each study, the raw sequencing reads were acquired as fastq files from the NCBI Sequence Read Archive and processed with the Qiime2 platform v2020.2 (9). Amplicon sequence variants (ASVs) were resolved with the dada2 pipeline

(10) and classified with a naïve Bayes classifier pre-trained on the Silva 138 SSU database (11-13). Reads for all individuals were rarefied to a uniform read depth matching the lowest read depth from a given individual in the study using the vegan package in R (14).

Table 2.1 Published datasets used in this analysis. Table denoting host animal species, number of individuals sampled, body site sampled, and PubMed Identification number (PMID).

Host	Number of Individuals	Body Sites Sampled	Reference
Mylossoma duriventre	45	Surface swab midgut, hindgut	Sylvain et al. 2020 PMID 32503908
Serrasalmus rhombeus	33	Surface swab, midgut, hindgut	Sylvain et al. 2020 PMID 32503908
Mesonata festivus	33	Surface swab, midgut, hindgut	Sylvain et al. 2020 PMID 32503908
Varanus komodoensis	34	Feces, skin	Hyde et al. 2016 PMID 27822543
Salmo salar	74	Fish surface, whole intestine	Webster et al. 2018 PMID 29915104
Euphasia superba	22	Moult, faeces	Clark et al. 2019 PMID 30697197
Plethodon glutinosus	60	Surface swab, faeces	Walker et al. 2019 PMID 31802185
Rhinolophus eloquens	23	Multiple body site skin swab (pooled), distal colon	Lutz et al. 2019, PMID 31719140
Miniopterus natalensis	26	Multiple body site skin swab (pooled), distal colon	Lutz et al. 2019, PMID 31719140
Rhinolophus clivosus	21	Multiple body site skin swab (pooled), distal colon	Lutz et al. 2019, PMID 31719140
Hipposideros caffer	34	Multiple body site skin swab (pooled), distal colon	Lutz et al. 2019, PMID 31719140
Hipposideros ruber	20	Multiple body site skin swab (pooled), distal colon	Lutz et al. 2019, PMID 31719140
Otomops harrissoni	25	Multiple body site skin swab (pooled), distal colon	Lutz et al. 2019, PMID 31719140
Miniopterus africanus	22	Multiple body site skin swab (pooled), distal colon	Lutz et al. 2019, PMID 31719140
Rousettus lanosus	31	Multiple body site skin swab (pooled), distal colon	Lutz et al. 2019, PMID 31719140
Homo sapiens	38	Multiple body sites (variable), faeces	Younge et al. 2018, PMID 29855335

Neutral Model Fitting

To determine the relative contribution of neutral processes to microbiome assembly, we assessed the fit of the Sloan Neutral Community Model for Prokaryotes (SNCM) (15) to the distribution of microbial taxa in the processed read datasets as previously described (8). SNCM fits were conducted for each host species, both skin/scale and gut microbiome communities. SNCM fit was primarily assessed by the root mean squared error (rmse) metric with lesser rmse values indicating a better fit of the SNCM to the data. 95% confidence intervals were constructed around the rmse values by fitting the model to a given sequencing dataset 1000 times, recording the rmse value for each model fit, and then computing the 95^{th} percentile of those values.

Simulations of neutral communities

I leveraged an existing neutral community simulation framework previously published (16) to simulate neutral microbiome communities. Simulations were conducted in python for 10^6 time steps to achieve steady-state neutral conditions. Simulations were constructed to recapitulate neutral processes described earlier (stochastic birth, death and migration). Demographic parameters (population size, diversity) were set to match the empirical community that was being simulated. The SNCM was then fit to the simulated communities in the same way as previously described.

Model Partition Analysis

Relative frequencies of ASVs located in the above, within or below partitions of SNCM predictions was computed for each of the SNCM fits for each host by dividing the number of ASVs in each partition by the total number of ASVs.

Results

I first compared the fit of the neutral model for microbial taxa (ASVs) in gut and skin or scale tissues separately for each host species with the metacommunity restricted to samples of the same tissue type. Model fit was assessed by the root mean squared error (rmse) metric with lesser rmse values indicating a better fit of the SNCM to the data. Across nearly all animal hosts, skin or scale microbiomes were equally or better fit to the neutral model compared to gut microbiomes (Figure 2.1A). These results suggest that overall, the assembly of microbiomes associated with skin or scale tissues tend to be more governed by neutral processes than gut microbiomes. However, the strength of this pattern varied among host taxonomic groups; for example, the fit of the neutral model did not differ between skin or scale and gut tissues for the fish datasets considered in this study, while skin microbiomes tended to be a better fit to the neutral model than gut microbiomes for mammal hosts.

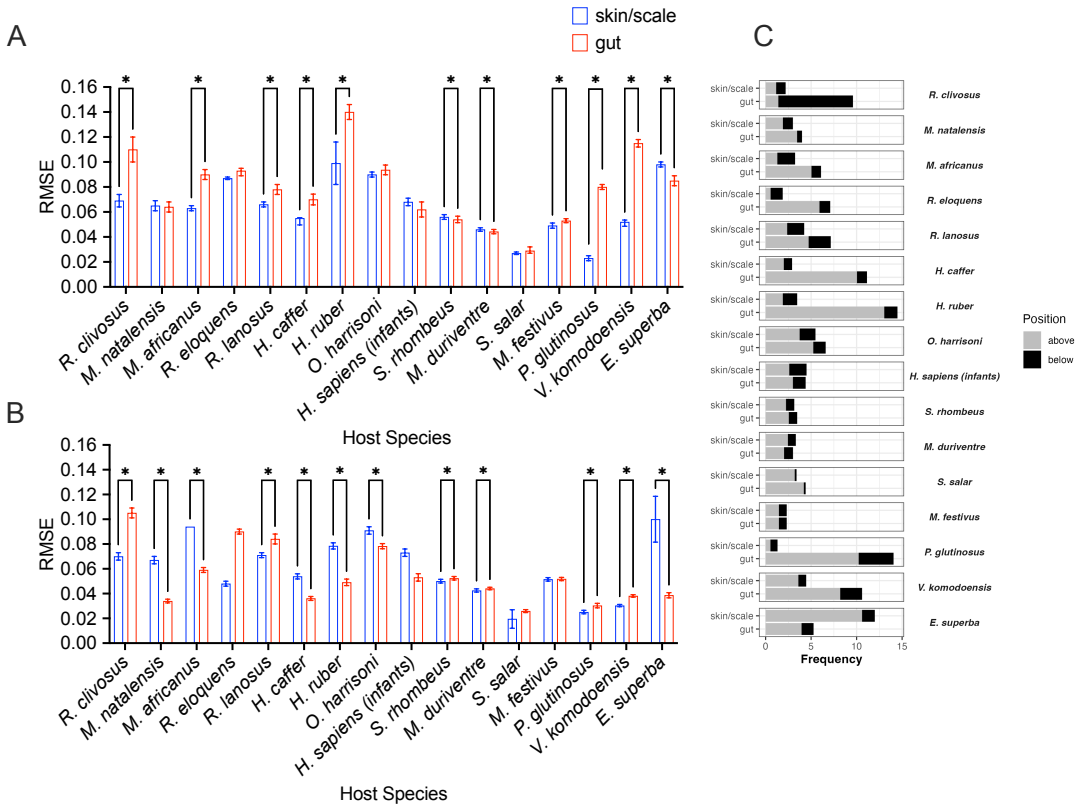

Figure 2.1 Neutral model fits to empirical and simulated microbiomes A) Neutral model fits of empirical microbial communities for both skin/scale and gut microbial communities across animal hosts. B) Neutral model fits of simulated microbial communities for both skin and scale and gut microbial communities based on community metrics obtained from corresponding empirical data. Error bars for both A and B represent 95% confidence intervals based on bootstrapping of data. C) Proportion of microbial taxa that fell outside of neutral model predictions for skin/scale and gut communities. Asterisks denote significance of $p < 0.05$ by detection with a paired t-test.

To better understand the factors that contribute to the observed patterns of neutrality in skin/scale vs. gut communities, we looked for patterns in the percentage of microbial taxa that fell outside of neutral model predictions across the different hosts for each tissue type. Taxa that occur more or less frequently than neutral model predictions are thought to be non-neutrally distributed and therefore may be subject to selective processes (Figure 2.1C). For example, taxa that occur in more individual hosts than predicted by the neutral model (above the neutral model

prediction) may be adapted to persist in the host environment or selected for by the host. In contrast, taxa below the neutral model prediction (i.e. detected in fewer samples than predicted by the SNCM) could be particularly dispersal limited or may be selected against by the host immune system. For nearly all the datasets considered in this study, the majority of the 'non-neutral' ASVs fell into the "above partition", suggesting that these taxa are particularly host-adapted (Figure 2.1C). For the few host species where the SNCM was a better fit for the gut microbiome than the skin or scale microbiome, this was also primarily due to a higher proportion of taxa in the above partition, suggesting that for a minority of host species, the gut environment is favorable to more microbial taxa than the skin or scale environment.

Next, I sought to compare the neutral model fits of empirical communities with simulated microbial communities (Figure 2.1B). Simulating microbial communities allowed us to obtain a steady-state level of neutrality against which I could compare the empirical communities. This is crucial, as neutrality levels may vary over time. For example, variations in neutrality are sensitive to 'selective' factors that may be present at varying intensities at different points in time, including changes in host immunological state due to immune system development or pathogen exposure (17,18). I leveraged an existing simulation (16) framework to generate completely neutral communities that had the same number of hosts, microbial diversity and migration parameter 'm' as the model fits from each empirical dataset. Simulating communities recapitulated the trends in neutrality observed in the empirical communities. However, the model was not uniformly better fit to simulated communities, indicating that microbial community composition can vary over time, and that longitudinal sampling may be necessary to fully understand microbiome assembly (Figures 2.1A and 2.1B). Finally, we assessed whether changing the definition of the metacommunity to include microbes from both the skin or scale

tissues and gut tissues of a given species influenced the fit of the neutral model. Microbes have been shown to disperse among body sites within a host individual, which suggests that a less tissue-specific definition of the metacommunity may be more appropriate (19-21). Overall, the observation that assembly of gut microbiomes tended to be equally or less neutral than the assembly of microbiomes in skin or scale tissues is consistent whether the metacommunity is restricted to a particular tissue type or includes both tissue types (Figure 2.2). However, there were some exceptions (e.g. *E. superba*), suggesting that careful consideration of the source and sink communities is essential for an accurate assessment of the contribution of neutral process to the assembly of host-associated microbiomes.

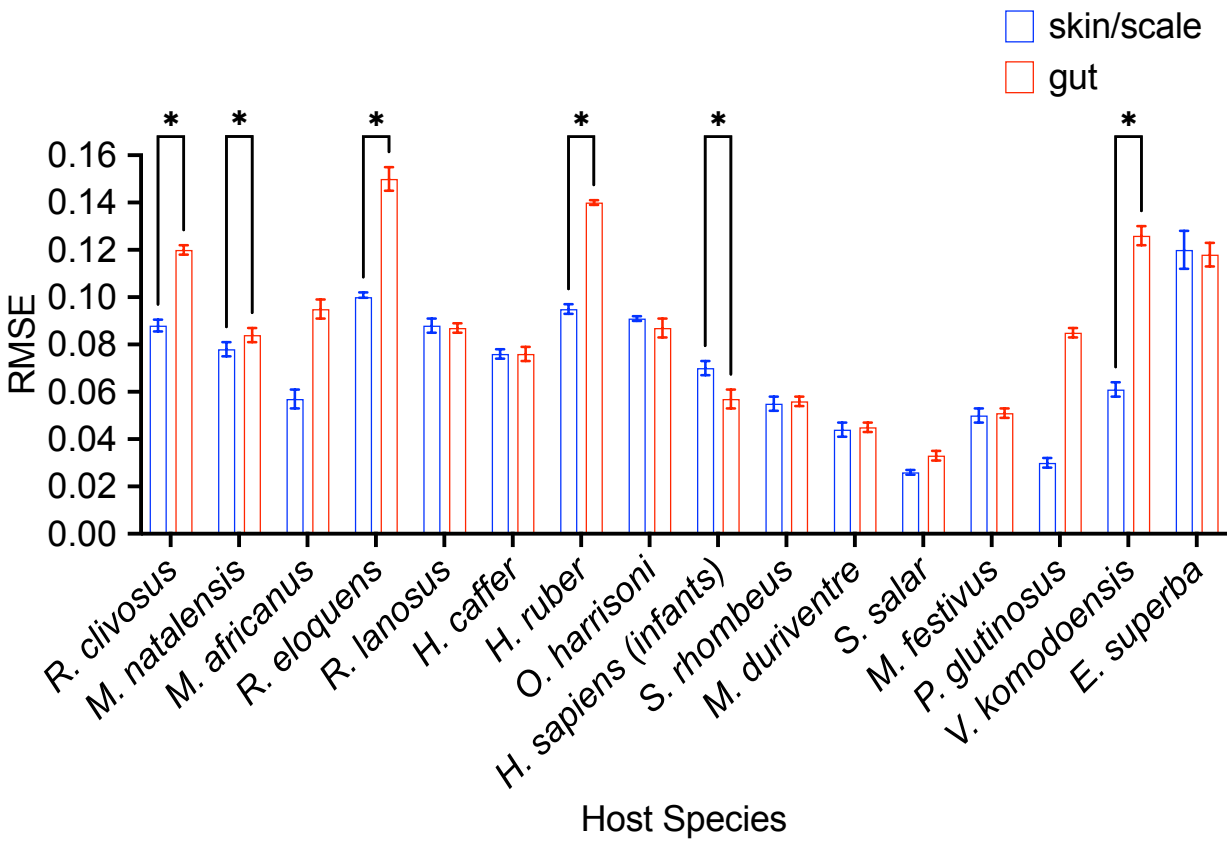

Figure 2.2: Neutral model fits of empirical microbial communities with the source pool of microbes defined to contain microbes from both tissue types. Error bars represent 95% confidence intervals generated by bootstrapping data. Asterisks denote significance of $p < 0.05$ by detection with a paired t-test.

Conclusion

In this study, I used a modelling-based approach to understand the ecological processes that underlie the assembly of microbiomes associated with gut and skin or scale tissues across a panel of animal hosts. This approach revealed that for the majority of animal species considered, the skin or scale microbiome was more neutrally assembled than the gut microbiome. This may be the result of variation among body sites in susceptibility to microbes dispersing from the environment or host activities that promote/deter microorganisms. We also noted variation among broad host taxonomic groups in the contribution of neutral processes to microbiome assembly among tissue types. Determining the factors that drive these differences (e.g. host lifestyle or immune system complexity) will be an important avenue of future research. Overall, our observations suggest that the gut environment tends to be more selective than the skin or scale environment and showcases the utility of this method to reveal potentially unique features of tissue environments in animal hosts

References

1. M. McFall-Ngai, M.G. Hadfield, T.C.G. Bosch, H.V. Carey, T. Domazet-Lošo, A.E. Douglas, N. Dubilier, G. Eberl, T. Fukami, S.F. Gilbert, U. Hentschel, N. King, S. Kjelleberg, A.H. Knoll, N. Kremer, S.K. Mazmanian, J.L. Metcalf, K. Nealson, N.E. Pierce, J.F. Rawls, A. Reid, E.G. Ruby, M. Rumpho, J.G. Sanders, D. Tautz, & J.J. Wernegreen, 2013. Animals in a bacterial world, a new imperative for the life sciences, Proc. Natl. Acad. Sci. U.S.A. 110 (9) 3229-3236,

2. Broderick, N. A., Buchon, N., & Lemaitre, B. (2014). Microbiota-induced changes in drosophila melanogaster host gene expression and gut morphology. *mBio*, *5*(3), e01117-14.

3. Perez Perez, G. I., Gao, Z., Jourdain, R., Ramirez, J., Gany, F., Clavaud, C., Demaude, J., Breton, L., & Blaser, M. J. (2016). Body Site Is a More Determinant Factor than Human Population Diversity in the Healthy Skin Microbiome. *PloS one*, *11*(4), e0151990.

4. Costello, E. K., Carlisle, E. M., Bik, E. M., Morowitz, M. J., & Relman, D. A. (2013). Microbiome assembly across multiple body sites in low-birthweight infants. *mBio*, *4*(6), e00782-13.

5. Faust K, Sathirapongsasuti JF, Izard J, Segata N, Gevers D, et al. 2012. Microbial Co-occurrence Relationships in the Human Microbiome. PLOS Computational Biology 8(7): e1002606.

6. Asangba AE,,Mugisha L,Rukundo J, Lewis RJ, Halajian A, Cortés-Ortiz L, Junge RE, Irwin MT, Karlson J, Perkin A, Watsa M,Erkenswick G,Bales KL, Patton DL, Jasinska AJ,Fernandez-Duque E, Leigh SR, Stumpf RM. 2022. Large Comparative Analyses of Primate Body Site Microbiomes Indicate that the Oral Microbiome Is Unique among All Body Sites and Conserved among Nonhuman Primates. Microbiol Spectr 10:e01643-21.

7. Vellend M. 2010. Conceptual synthesis in community ecology. *The Quarterly review of biology*, *85*(2), 183–206.

8. Burns, A. R., Stephens, W. Z., Stagaman, K., Wong, S., Rawls, J. F., Guillemin, K., & Bohannan, B. J. 2016. Contribution of neutral processes to the assembly of gut microbial communities in the zebrafish over host development. *The ISME journal*, *10*(3), 655–664.

9. Bolyen, E., Rideout, J. R., Dillon, M. R., Bokulich, N. A., Abnet, C. C., Al-Ghalith, G. A., Alexander, H., Alm, E. J., Arumugam, M., Asnicar, F., Bai, Y., Bisanz, J. E., Bittinger, K., Brejnrod, A., Brislawn, C. J., Brown, C. T., Callahan, B. J., Caraballo-Rodríguez, A. M., Chase, J., Cope, E. K., … Caporaso, J. G. (2019). Reproducible, interactive, scalable and extensible microbiome data science using QIIME 2. *Nature biotechnology*, *37*(8), 852–857.

10. Callahan, B. J., McMurdie, P. J., Rosen, M. J., Han, A. W., Johnson, A. J., & Holmes, S. P. 2016. DADA2: High-resolution sample inference from Illumina amplicon data. *Nature methods*, *13*(7), 581–583.

11. Bokulich, N. A., Kaehler, B. D., Rideout, J. R., Dillon, M., Bolyen, E., Knight, R., Huttley, G. A., & Gregory Caporaso, J. 2018. Optimizing taxonomic classification of marker-gene amplicon sequences with QIIME 2's q2-feature-classifier plugin. *Microbiome*, *6*(1), 90.

12. Pedregosa, F., Varoquaux, G., Gramfort, A., Michel, V., Thirion, B., Grisel, O., ... & Duchesnay, É. 2011. Scikit-learn: Machine learning in Python. *the Journal of machine Learning research*, *12*, 2825-2830.

13. Quast, C., Pruesse, E., Yilmaz, P., Gerken, J., Schweer, T., Yarza, P., Peplies, J., & Glöckner, F. O. 2013. The SILVA ribosomal RNA gene database project: improved

data processing and web-based tools. *Nucleic acids research*, *41*(Database issue), D590–D596.

14. Oksanen J, Simpson G, Blanchet F, Kindt R, Legendre P, Minchin P, O'Hara R, Solymos P, Stevens M, Szoecs E, Wagner H, Barbour M, Bedward M, Bolker B, Borcard D, Borman T, Carvalho G, Chirico M, De Caceres M, Durand S, Evangelista H, FitzJohn R, Friendly M, Furneaux B, Hannigan G, Hill M, Lahti L, Martino C, McGlinn D, Ouellette M, Ribeiro Cunha E, Smith T, Stier A, Ter Braak C, Weedon J 2022. *vegan: Community Ecology Package*. R package version 2.6-4, https://vegandevs.github.io/vegan/.

15. Sloan, W. T., Lunn, M., Woodcock, S., Head, I. M., Nee, S., & Curtis, T. P. 2006. Quantifying the roles of immigration and chance in shaping prokaryote community structure. *Environmental microbiology*, *8*(4), 732–740.

16. Sieber, M., Pita, L., Weiland-Bräuer, N., Dirksen, P., Wang, J., Mortzfeld, B., Franzenburg, S., Schmitz, R. A., Baines, J. F., Fraune, S., Hentschel, U., Schulenburg, H., Bosch, T. C. G., & Traulsen, A. 2019. Neutrality in the Metaorganism. *PLoS biology*, *17*(6), e3000298.

17. Stephens WZ, Burns AR, Stagaman K, Wong S, Rawls JF, Guillemin K, Bohannan BJ. The composition of the zebrafish intestinal microbial community varies across development. ISME J. 2016 Mar;10(3):644-54. doi: 10.1038/ismej. 2015.140. Epub 2015 Sep 4. PMID: 26339860; PMCID: PMC4817687.

18. Jani, A. J., Bushell, J., Arisdakessian, C. G., Belcaid, M., Boiano, D. M., Brown, C., & Knapp, R. A. 2021. The amphibian microbiome exhibits poor resilience following pathogen-induced disturbance. *The ISME journal*, *15*(6), 1628–1640.

19. Custer, G. F., Bresciani, L., & Dini-Andreote, F. 2022. Ecological and Evolutionary Implications of Microbial Dispersal. *Frontiers in microbiology*, *13*, 855859.

20. She, J. J., Liu, W. X., Ding, X. M., Guo, G., Han, J., Shi, F. Y., Lau, H. C., Ding, C. G., Xue, W. J., Shi, W., Liu, G. X., Zhang, Z., Hu, C. H., Chen, Y., Wong, C. C., & Yu, J. 2024. Defining the biogeographical map and potential bacterial translocation of microbiome in human 'surface organs'. *Nature communications*, *15*(1), 427.

21. Venkataraman, A., Bassis, C. M., Beck, J. M., Young, V. B., Curtis, J. L., Huffnagle, G. B., & Schmidt, T. M. 2015. Application of a neutral community model to assess structuring of the human lung microbiome. *mBio*, *6*(1), e02284-14. https://doi.org/10.1128/mBio.02284-14

CHAPTER III

EVOLUTION OF POLYAMINE RESISTANCE IN STAPHYLOCOCCUS AUREUS THROUGH MODULATION OF POTASSIUM TRANSPORT

From: Campbell, Kowalski, Kohler, Kebret and Barber. 2025. Evolution of polyamine resistance through modulation of potassium transport. mSphere 0:e00613-24.

This chapter was published in mSphere. This project arose as a series of conversations between myself, Matt Barber and Caitlin Kowalski.

Introduction

Staphylococcus aureus is a Gram-positive bacterium that colonizes approximately 30% of the human population as well as human-associated animals (1, 2). *S. aureus* is most frequently isolated from the anterior nares, where it resides as a commensal member of the human microbiota (3, 4). However, *S. aureus* is also capable of colonizing the skin and is a leading cause of soft skin and tissue infections (SSTIs) as well as other invasive conditions including bloodstream infections, pneumonia, osteomyelitis, and endocarditis (4–8). *S. aureus* is a frequent agent of antibiotic-resistant infections, with methicillin resistant *S. aureus* (MRSA) causing between 10,000 and 20,000 deaths in the United States annually (8, 9). Recent global estimates indicate that *S. aureus* is a leading cause of both total bacterial infections and antibiotic resistant infections in humans across geographic and socioeconomic boundaries (10, 11).

Previous studies have identified a number of biotic and abiotic factors that limit *S. aureus* colonization in distinct host niches (12–15). In particular, polyamines are an abundant class of aliphatic cationic molecules known to restrict *S. aureus* growth during infection (16, 17).

Polyamines are characterized by the presence of at least two primary amino groups and include putrescine, agmatine, spermidine, and spermine (18, 19). Polyamines are byproducts of arginine metabolism and are synthesized by different series of enzymatic steps depending on the organism (20). Polyamine metabolism and functions are well-studied in eukaryotes, where they play pleiotropic roles in cellular physiology (21–23). Due to their net positive charge, polyamines are capable of binding to ribosomes and DNA during translation and DNA replication, respectively (18, 24). In mammals, the enzymes that produce and breakdown polyamines are controlled at multiple transcriptional levels, resulting in a tightly-regulated pool of polyamines within a cell at any given time (19, 25).

Given the numerous roles that polyamines play in essential cellular functions, polyamine synthesis was once believed to be conserved across the entire tree of life (26). This dogma was overturned by work demonstrating that multiple bacterial genera have lost the ability to synthesize polyamines *de novo* (21). Even among bacteria that do not synthesize polyamines, supplementing media with exogenous polyamines often results in modest growth improvement (27, 28). In marked contrast to other bacteria, polyamines are highly bactericidal to most *Staphylococcus* species with particularly potent effects on *S. aureus* (16). A key exception are *S. aureus* strains within the USA300 lineage, which exhibit enhanced polyamine resistance (28, 29). USA300 defines a lineage of community-acquired MRSA (CA-MRSA) that emerged in the early 2000s that has since spread to epidemic levels (29). The discovery of the arginine-catabolic mobile element (ACME) unique to USA300 provided a key genetic determinant that has likely contributed to the rise of this lineage (28–30). ACME is an approximately 31 kilobase (kb) genomic island that contains at least 33 putative genes (28, 29). Evidence suggests that ACME was assembled in *Staphylococcus epidermidis* and then horizontally transferred to the most

recent common ancestor of USA300 (28). Notably, ACME contains a spermine acetyltransferase gene, *speG*, which is sufficient to confer resistance to polyamines (16, 28). While acetyltransferase activity of *speG* is required for polyamine resistance (16), how acetylation of polyamines reduces their toxicity to *S. aureus* remains unresolved.

The ACME locus contains several genes related to arginine metabolism, which produce ammonia allowing these strains to efficiently colonize and infect the acidic environment of the skin (16, 28, 29, 31). At present, the basis of polyamine toxicity and mechanisms by which non-USA300 *S. aureus* may adapt to these molecules are largely unknown. While ACME and *speG* in particular provide an example of how polyamine resistance may evolve, alternative genetic or molecular mechanisms of resistance have not been well-characterized. To address this question, I experimentally evolved populations of *S. aureus* under increasing concentrations of spermine and surveyed the consequences of resistance evolution across three different strain backgrounds. My findings identify new genes and mechanisms contributing to polyamine resistance in this major bacterial pathogen.

Materials and Methods

Strains

All strains used in the experimental evolution experiment were acquired from BEI resources. *Ktr* mutants were generated for the purposes of this study following an allelic exchange protocol described below.

Experimental evolution

Glycerol stocks of each strain were struck out on to tryptic soy agar (BD) plates and incubated overnight at 37° C. For each strain, a total of 6 single colonies were picked, and each colony was used to inoculate a separate 3 mL culture containing tryptic soy broth (TSB) (BD). These liquid cultures were grown overnight for approximately 18 hours, shaking (225 rpm) at 37° C. Each liquid culture was used to initiate a replicate population in the evolution experiment. Four of the cultures were diluted 1/100 into fresh TSB containing 2mM of spermine (Sigma, 71-44-3), and two of the cultures were diluted 1/100 into plain TSB as a control. After passaging, the populations were returned to the shaking incubator. The populations were passaged daily in the same 1/100 dilution throughout the course of the experiment. Populations initially exposed to spermine on the first passaged were continuously exposed to increasing concentrations of spermine for the remainder of the evolution experiment. Control populations were passaged daily in plain TSB. Populations were sampled and frozen in a glycerol solution (25% final v/v) at passage 0, 4, 6, 8, and 10.

DNA isolation and sequencing

Whole bacterial populations were sequenced that were exposed to spermine during the experiment, as well as the control populations that were never exposed to spermine. All four replicates of *S. aureus* MN8 populations were sequenced at passages 4, 6, 8 and 10. All four replicate populations of *S. aureus* HFH-30364 and *S. aureus* RN4850 that were exposed to spermine were sequenced at passage 10. For all experimentally evolved populations, ancestral clones for each strain that were used to initiate the evolution experiments were sequenced to provide a reference genome for variant calling. We also sequenced the two control populations

(never exposed to spermine) for each strain background at passage 10. To isolate DNA, populations were struck out on to TSA plates from glycerol stocks, and mixed-colony samples were taken liberally from all parts of the plate to capture any diversity potentially present in the population. Bacterial samples were resuspended in TE buffer containing 50 µg/mL lysostaphin and incubated for one hour to facilitate lysis of cells. DNA was then harvested using a Qiagen DNeasy blood and tissue kit (CAT# 69504) according to manufacturer's instructions. DNA extracts were sent to SeqCenter (seqcenter.com) for Illumina sequencing.

Data processing and variant calling

Mutations in the evolved populations were identified with breseq v0.35.7 (55) using the default settings and polymorphism mode to calculate the frequencies of variants detected in the reads. Polymorphism mode in breseq calls a variant in the population if it is observed in both strands of at least 5% of the reads. The average read depth for MN8, HFH-30364, and RN4850 populations were 439x, 410x, and 600x respectively. Average genome coverage for MN8, HFH-30364 and RN4850 was 99.1%, 99.8%, and 99.5% respectively.

Minimum inhibitory concentration measurements

Minimum inhibitory concentration (MIC) experiments were conducted using a modified broth microdilution method. To measure the MIC of a given compound, a single colony of bacteria was picked and inoculated into 4 mL of TSB to start overnight cultures. The next day, the OD600 of the cultures was measured and diluted to an OD600 of 0.04. Different concentrations of an antimicrobial compound of interest (e.g. spermine) were made by diluting stocks of the chemical in 2X TSB and water, yielding the final concentrations of the compound

in 1X TSB. 50 µL of diluted overnight culture was mixed 1:1 with each concentration of the prepared antimicrobial agent. Mixtures of bacterial cultures and antimicrobial compounds were incubated statically in 96 well plates at 37 °C for 24 hours. MIC values were determined as a range between the highest concentration at which visible growth occurred, and the lowest concentration at which no visible growth occurred. Bacteria were challenged at each concentration in triplicate, and the results reported are the average of three individual experiments.

Protein modelling and mutation mapping

Published protein structures (PDB ID: 4J7C) and genetic sequences for the *Bacillus subtilis* KtrAB complex were used as guides to model the structure of the *S. aureus* KtrAD protein complex in ChimeraX (version 1.6.1).

Generation of S. aureus mutants

To generate single base-pair (bp) mutations, allelic exchange was used with the pIMAY vector following protocols previously described (56). PCR products containing sequence approximately 1,000 bp upstream and downstream of the mutation of interest were generated. Primers were designed containing homology arms to facilitate assembly into the cloning vector. Genomic DNA extracted from the evolved MN8 isolates was used as template DNA to amplify the mutations of interest. PCR products were assembled into a digested pIMAY vector using NEBuilder HiFi DNA assembly (CAT# E2621S) according to the manufacturer's instructions. Assembled vectors were chemically-transformed into *E. coli* DC10B and plated on to TSA + 25 µg/mL chloramphenicol to select for successful transformants. Colonies were screened with

colony PCR to confirm presence of insert gene into pIMAY vector. Validated plasmids were isolated and electroporated into recipient *S. aureus* strains as described previously (57). Transformed *S. aureus* cells were plated on to TSA + 10 μg/mL chloramphenicol at 28 C overnight. Single colonies were picked re-plated on to TSA + 10 μg/mL chloramphenicol to select for a single recombination event. Single colonies that grew on chloramphenicol were picked, grown up overnight in plain TSB, and then plated on to TSA + 1 μg/mL anhydrotetracycline (atc) to select for loss of the plasmid backbone. Successful secondary recombinants would be permissive to growth on atc. Single colonies that could grow on atc were picked and sequenced at the locus of interest to confirm that the mutation of interest was introduced successfully.

Cytochrome C binding assay

Relative cell surface charge was determined by measuring cytochrome C binding as described previously (58). Stationary phase overnight cultures were harvested and adjusted to an OD_{600} of ~1.1 in 2mL of sodium acetate buffer (20 mM, pH 4.6). Cultures were washed twice in sodium acetate buffer before being resuspended in 0.5mL sodium acetate buffer with 0.25 mg/mL cytochrome C. Resuspended pellets were incubated while shaking at 37 °C for 15 minutes, then centrifuged at 16000 x g for 2 minutes. The supernatant was removed and aliquoted into 96 well plates, where the absorbance was measured at 410 nm using a Biotek plate reader. The percentage of cytochrome C bound for a given sample was calculated as the fraction of absorbance relative to 0.25 mg/mL cytochrome C in sodium acetate buffer alone.

Membrane potential measurements

Membrane potential was assessed using DiSC3(5) (MedChem Express #HY-D0085-25mg) and a Biotek plate reader according to previously published methods (59). Cells were grown overnight to stationary phase, at which point they were diluted to an OD600 of 0.3. Cells were then incubated in 100 uL volumes in a black polystyrene 96-well plate with 5 uM DiSC3(5) for 3 minutes before being transferred to the plate reader. For cells treated with gramicidin, 1 uM gramicidin was added after the three-minute incubation of DiSC3(5), then read in the plate reader. Fluorescence was read in the plate reader at 610 nm excitation and 660 nm emission. Readings were conducted every 2.5 minutes for 1 hour. Arbitrary fluorescence units were calculated as by dividing the fluorescence measurement by the OD600 of the cells.

Chemically defined media lacking excess potassium

To measure the effect of specific amounts of potassium in the growth media, we constructed chemically defined media lacking excess potassium as described previously (37). Defined amounts of potassium were added into the media by the addition KCl. Survival assays were conducted at different KCl concentrations as described below.

Survival assays

Overnight cultures were harvested, adjusted to a desired OD600 and incubated with an antibacterial compound of interest following the same protocol described above for MIC assays. Bacterial survival in various compounds was measured by plating and enumerating CFUs over the course of 24 hours of static incubation at 37 °C.

Results

Experimental evolution of spermine resistance in S. aureus

To identify mechanisms of polyamine resistance in *S. aureus*, we performed a serial-passaging experiment in which populations of *S. aureus* were continuously exposed to increasing concentrations of spermine (Figure 2.1A, Table 2.1). Initially, single colonies of *S. aureus* strains MN8, HFH-30364, and RN4850 were revived from glycerol stocks on tryptic soy agar (TSA) plates. Both *S. aureus* MN8 and RN4850 are methicillin sensitive strains while HFH-30364 is a MRSA isolate from the USA400 lineage (Table 1). Replicate populations of each strain were then inoculated in tryptic soy broth media (TSB) to perform the passaging experiment. Spermine was selected as a representative polyamine as it has a well-documented bactericidal effect on *S. aureus* (16) and is abundant during the post-inflammatory phase of wound healing in murine models (17). Each day, a 1/100 aliquot of each replicate culture was transferred to fresh TSB with a pre-determined concentration of spermine (or no spermine for the control populations). Populations were initially exposed to sub-inhibitory conditions of spermine (2 mM) and passaged daily for 10 days, until reaching a final concentration of 7 mM spermine. Genomic DNA was collected to perform whole-population sequencing of MN8 samples taken throughout the evolution experiment. For RN4850 and HFH-30364, we conducted whole-genome, population-level sequencing upon completion of the passaging experiment (Figure 3.1A).

We observed that all populations in each of the three strain backgrounds evolved increased spermine resistance within 10 passages of laboratory evolution. Specifically, both *S. aureus* MN8 and HFH-30364 populations evolved levels of resistance at least 4-fold greater than the minimal inhibitory concentration (MIC) of the ancestral strain (Figure 3.1B). *S. aureus*

RN4850 exhibited a more variable resistance profile, with most replicate populations evolving an MIC nearly four times the ancestral levels (Figure 3.1B). Individual colonies tested from each population displayed slight differences in spermine resistance, likely reflecting heterogeneity in mutations carried by individual clones. *S. aureus* MN8 displayed the largest fold-change in spermine MIC, with individual colonies measuring between 5-6X the ancestral MIC levels (Figure 3.1B). We noted that the dynamics of resistance evolution as measured by spermine MIC varied between strain backgrounds. *S. aureus* MN8 gradually evolved increased resistance throughout the passaging experiment, while HFH-30364 experienced a single, large increase in resistance change between passages 0-4, and RN4850 experienced two large increases in resistance from passage 0-4 and passage 8-10 (Figure 3.1B). Together these results reveal that *S. aureus* can readily evolve resistance to spermine under laboratory conditions, while the dynamics of resistance evolution differ between strain backgrounds (Figure 3.1B). Given that *S. aureus* MN8 populations evolved the highest magnitude change of resistance relative to the ancestor, we chose to focus on characterizing the genetic basis of spermine resistance in this strain background for future experiments.

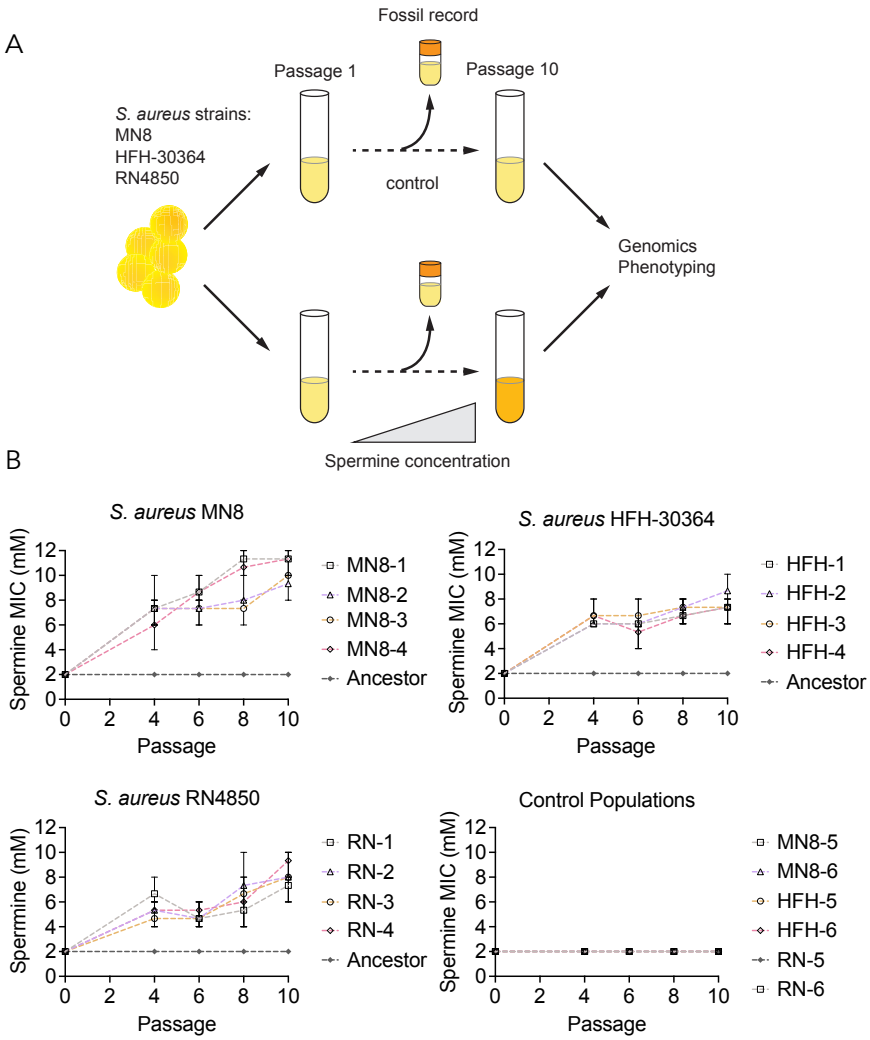

Figure 3.1: Experimental evolution of spermine resistance in *Staphylococcus aureus*. **A**. Experimental evolution overview. Populations of each strain of *S. aureus* (MN8, HFH-30364, and RN4850) were revived from glycerol stocks on to tryptic soy agar (TSA). For each strain background, four single colonies were picked to establish replicate populations to undergo exposure to spermine and two colonies were picked to establish replicate control lines to be passaged in TSB alone. Populations were passaged at a fixed dilution daily, and spermine-exposed lines were continuously exposed to spermine. Glycerol stocks containing aliquots of the evolving populations were saved periodically as a "fossil record." At the end of the experiment, glycerol stocks were revived to perform phenotypic analyses and to isolate DNA for sequencing. **B.** Spermine minimal inhibitory concentration (MIC) was calculated over the course of the evolution experiment. Glycerol stocks from throughout the experiment were revived on TSA plates, then single colonies were picked and spermine MIC was measured. Shapes and error bars

represent average and range of MIC values measured. Each point represents the average of a separate experiment conducted in triplicate.

Genetic determinants of spermine resistance

We next sought to determine the genetic basis of polyamine resistance in our evolved *S. aureus* populations. Whole-population DNA samples were extracted from each replicate population throughout the experiment (MN8) and at the end of the passaging experiment (HFH-30364, RN4850). Additionally, we extracted DNA from ancestral clones to generate a reference sequence for variant calling. *S. aureus* MN8 populations exhibited striking evidence of convergent evolution, with three of the four spermine-exposed populations harboring mutations in different components of the *ktr* potassium transport complex (Table 1). The Ktr system has been characterized in *Bacillus subtilis* as a constitutively expressed moderate-affinity potassium transporting system, and has only recently been described in *S. aureus* (32, 33). This complex is composed of three proteins: KtrA, which forms a regulatory octameric ring subunit in the cytoplasm, and two redundant, ion conducting proteins: KtrB and KtrD. Each are dimeric transmembrane channels that facilitates potassium import. KtrB or KtrD in combination with KtrA are required to form a functional complex. Previous work has implicated the Ktr complex in both osmotic and alkaline stress tolerance (32–34). The Ktr complex also contributes to survival against a variety of antibacterial agents under low potassium conditions, as Δ*ktrA* deletion mutants possess increased sensitivity to aminoglycoside antibiotics (32, 33). Despite this, no study to date has directly linked Ktr complex function and polyamine resistance.

Table 3.1. Mutations observed during experimental evolution.
A subset of mutations that arose in each lineage of each strain background during the evolution experiment. Mutations reported were detected using breseq from while genome sequencing from DNA isolated at passage 10 of the evolution experiment.

Population	*ktr* potassium transport complex		ATP-synthase machinery			
	ktrA	***ktrD***	***atpG***	***atpA***	***atpH***	***pgl***
MN8-1	E76G	Q450K, S135L				
MN8-2						
MN8-3	E76G	M391I				
MN8-4	A178V	G94C				
HFH-1				P95L		G4E, H306Y
HFH-2	E151V		T242P			G108V
HFH-3						G287V, G323D
HFH-4						G4E, G120S, R318S
RN-1						A245V, T10P
RN-2			Δ69 bp			P234L, S41F, G261E, H138Y, F268V
RN-3			L261*			A245V
RN-4					Q170*	

MN8-derived populations exhibited the highest levels of polyamine resistance of the three strain backgrounds tested and were the only populations carrying high-frequency mutations in *ktr* genes (Table 1). We were therefore motivated to further investigate the evolutionary dynamics of spermine resistance in the MN8 populations. We leveraged whole-genome, whole-population sequencing to track the frequencies of *ktr* mutations over time. In each of the three replicate populations containing *ktr* mutations (MN8-1, MN8-3, MN8-4), nonsynonymous mutations occurred in both *ktrA* and *ktrD* at high frequencies by the final passage (Figure 3.2). Specifically, a single nonsynonymous mutation in *ktrA* had fixed by passage 10 in replicate

populations MN8-1 and MN8-4, and had nearly fixed in MN8-3 (84% allele frequency) (Figure 3.2A, 3.2C).

Notably, only a *single ktrA* allele was maintained in in any of the populations by the final passage, whereas multiple *ktrD* alleles co-occurred in both MN8-1 and MN8-3 (Figure 3.2A, 3.2B). The allele frequency dynamics were also different throughout each of the replicate populations. Single mutations in *ktrA* and *ktrD* arose early and fixed in MN8-4 by passage 6 (Figure 3.2C). However, the dynamics for MN8-1 and MN8-3 were more varied. In MN8-1, a single mutation in *ktrA* largely persisted until passage 8, when multiple *ktrD* mutations were detected in the population at low frequencies (Figure 3.2A. 3.2B). MN8-3 displayed similar characteristics to MN8-4, in which all *ktr* mutations arose late in the experiment between passages 8 and 10 (Figure 3.2B, 3.2C). We next picked multiple clones from the terminal passage in both MN8-1 and MN8-3 to determine the linkage of these *ktr* mutations. While multiple mutations were present in the *ktrD* gene in MN8-1, they existed in different lineages and always in combination with the *ktrA* mutation (Figure 3.2A). This was also true in MN8-3, where a single mutation in *ktrD* was found in combination with a single mutation in *ktrA* (Figure 3.2B). Despite multiple *ktrD* mutations existing at the population level, we did not detect any lineages within MN8-3 carrying multiple *ktrD* mutations (Figure 3.2B). Our findings suggest that resistance to spermine was largely conferred through a combination of single mutations in both *ktrA* and *ktrD.*

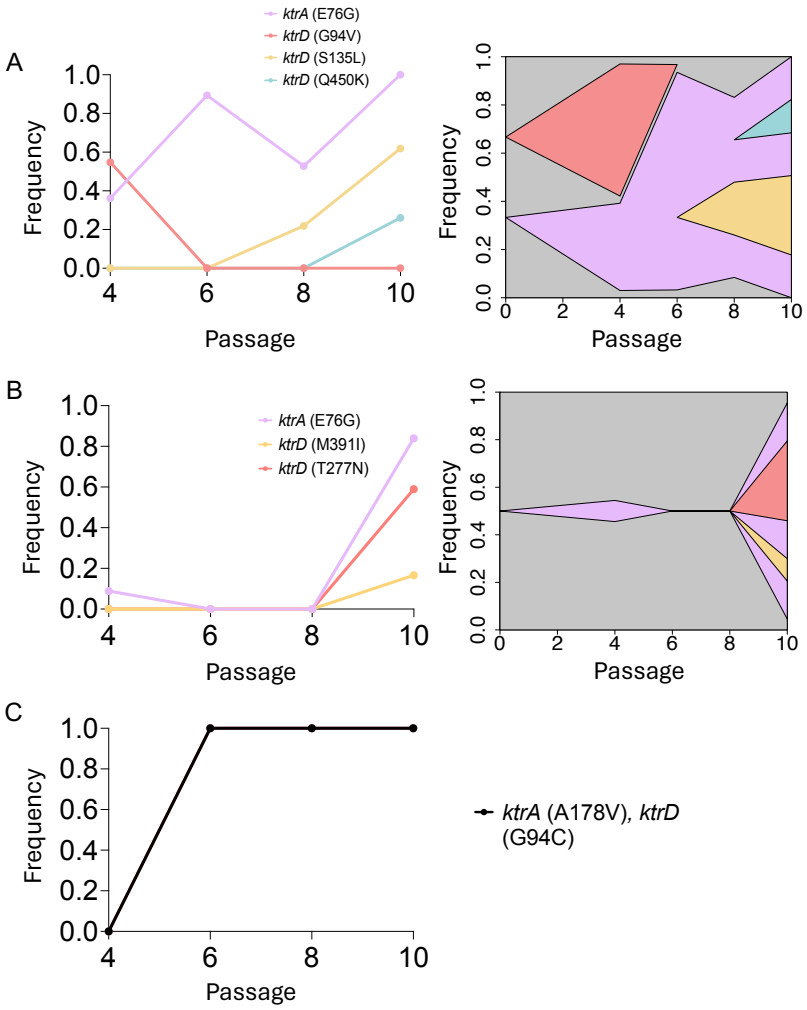

Figure 3.2. Allele frequency dynamics and linkage of *ktr* mutations over the course of experimental evolution. Allele frequencies and linkage were determined for *ktrA* and *ktrD* mutations in the MN8-1 (**A**), MN8-3 (**B**), and MN8-4 (**C**) populations. For all allele frequency line plots, breseq was run in polymorphism mode to determine the frequency of *ktrA* and *ktrD* single nucleotide polymorphisms (SNPs) detected in the population throughout the evolution experiment. To determine the linkage of *ktr* alleles present in each population, a combination of PCR and Sanger sequencing was used. For both MN8-1 and MN8-3, 16 different colonies were picked and colony PCR was conducted on both the *ktrA* and *ktrD* locus for each colony. PCR products were sent for Sanger sequencing, and sequences were aligned to detect which SNPs were present in each clone. Sanger sequencing revealed that clones in both MN8-1 and MN8-3 could contain a single SNP in *ktrD* on the background of a single SNP in *ktrA*

Single amino acid changes in ktr genes confer additive polyamine resistance

To determine whether single mutations in *ktr* genes are sufficient to confer spermine resistance in *S. aureus*, we generated targeted mutations in both *ktrA* and *ktrD* by homologous recombination in strain MN8. Specifically, the histidine at position 47 of KtrA was substituted for a tyrosine (H47Y), and the glycine at position 94 of KtrD was substituted for a valine (G94V) (Figure 3.2A). These mutations were recovered during a pilot evolution experiment performed as described in Figure 3.1 (Table S3.2) and are in proximity to mutations recovered in the evolution experiments described above. We then measured spermine MIC of each single mutant, as well as the *ktrA/ktrD* double mutant. We found that each single mutation conferred partial resistance to spermine, with an MIC of 6-8 mM for both the KtrA H47Y and KtrD G94V alleles (Figure 3.3B). However, the *ktrA/ktrD* double mutant conferred a similar level of resistance to spermine that we observed at the final passage of our evolution experiment (7 mM), making this combination of mutations sufficient to provide the level of resistance observed in these populations (Figure 3.3B). Together these results demonstrate that evolved mutations in *ktrA* and *ktrD* are sufficient to confer polyamine resistance in *S. aureus* in an additive manner. We also confirmed the ability of these strains to survive spermine concentrations by enumerating colony forming units per milliliter of culture (CFU/mL) (Figure 3.3B). We observed a ~100-fold reduction in recovered CFUs for the ancestral strain when incubated for 24 hours in 4 mM spermine compared to the no spermine control. In contrast, there was no reduction in CFUs observed for either of the single mutants in 4 mM versus 0 mM spermine (Figure 3.3B). We similarly did not observe a significant reduction in CFU/mL for the *ktrA/ktrD* double mutant when incubated with 4mM or 8 mM spermine, reflecting the ability of single amino acid changes to confer additive spermine resistance (Figure 3.3B). Notably, deletion of either *ktrA* or *ktrD* did

not alter spermine susceptibility relative to the ancestral MN8 strain (Figure 3.3B), indicating that the evolved nonsynonymous mutations do not function as null alleles. Together these experiments demonstrate that evolved *ktrA* and *ktrD* alleles are sufficient to confer polyamine resistance in *S. aureus.*

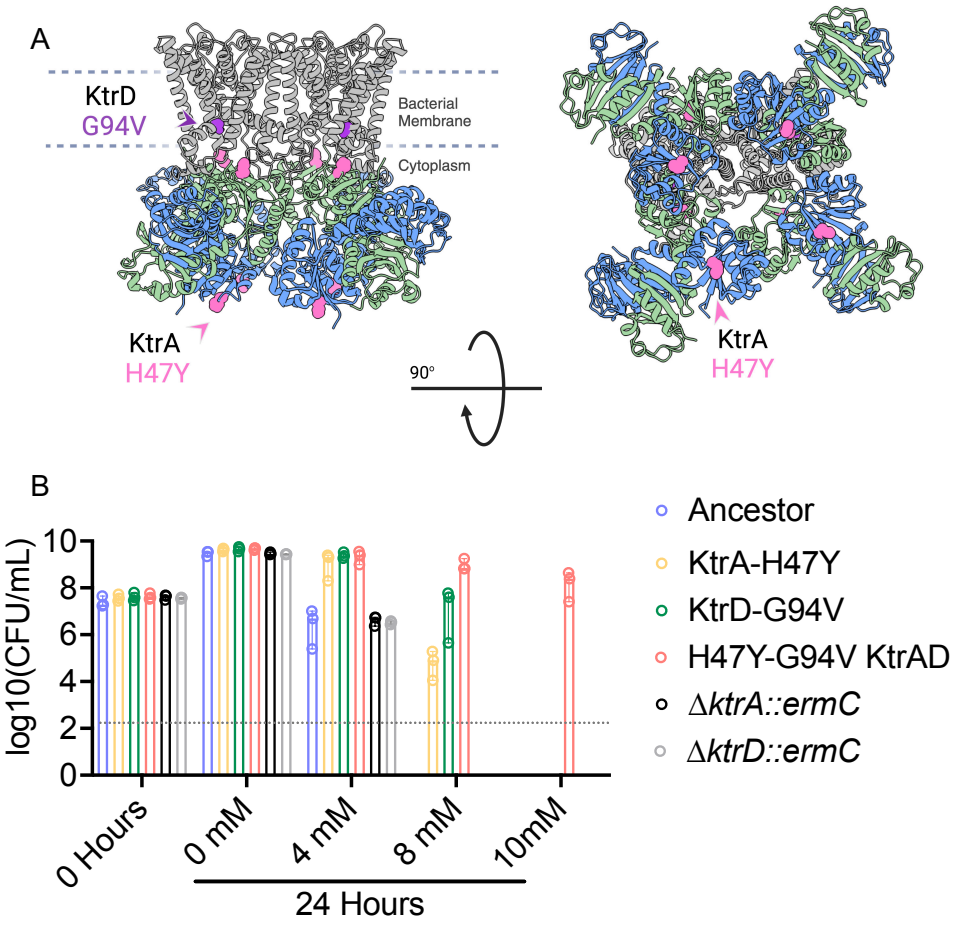

Genotype	Spermine MIC
Ancestral	2-4 mM
KtrA-H47Y	6-8 mM
KtrD-G94V	6-8 mM
H47Y-G94V KtrAD	10-12 mM
Δ*ktrA::ermC*	2-4 mM
Δ*ktrD::ermC*	2-4 mM

Figure 3.3 Evolved mutations in the KtrAD complex confer additive spermine resistance in *S. aureus*. Predicted structure of the KtrAD complex generated using ChimeraX. *S. aureus ktrA* and *ktrD* gene sequences were used to model the KtrAD complex based on the published KtrAD crystal structure from *Bacillus subtilis* (PDB ID: 4J7C). Mutations introduced into the MN8 strain background are highlighted in pink (KtrA) and purple (KtrD). **B.** Colony forming units (CFUs) recovered from MN8 *S. aureus* strains incubated in different concentrations of spermine for 24 hours (top), with corresponding spermine MIC values listed in the table (bottom). Gray dotted line represents limit of detection.

Evolved ktr mutations alter S. aureus antibiotic susceptibility

Previous reports indicate that the *ktr* potassium transport system plays an important role in antimicrobial resistance and alkaline stress tolerance in *S. aureus* (33). We therefore sought to determine if our evolved *ktr* mutations also altered the ability of *S. aureus* to tolerate other stressors beyond spermine. We measured the change in MIC for a panel of antibiotics in strain MN8 as well as the engineered *ktrA* (H47Y) and *ktrD* (G94V) mutants (Figure 3.4A). Previous findings revealed that *ktr* null mutants sensitize *S. aureus* to aminoglycoside antibiotics (32). In contrast to null mutants, the evolved *ktrA/ktrD* double-mutant exhibits an approximately 12-fold increase in aminoglycoside MIC compared to the ancestor (Figure 3.4A). Aminoglycoside antibiotics rely upon an intact proton motive force to cross the *S. aureus* cell membrane, where they inhibit protein translation (35, 36). We therefore hypothesized that the *ktr* mutants identified through experimental evolution function by altering membrane potential and preventing aminoglycoside internalization. Potassium transport, and *ktr*-mediated potassium transport in particular, is known to regulate membrane potential (32, 37, 38). To address this hypothesis, we used the voltage-sensitive, membrane-permeable dye, $DiSC_3(5)$ that readily enters *S. aureus* cells in a polarized state. Depolarization of the cell membrane prevents efficient uptake of the dye. We detected a modestly depolarized membrane potential in the *ktr* double mutants compared to the ancestral strain (Figure 3.4B). Despite reproducible difference in membrane potential, we were not convinced that this was the only factor contributing to antimicrobial resistance in the *ktr* mutants due to effect size. Prior to internalization into the bacterial cell, aminoglycoside uptake is governed by electrostatic attraction between the positively-charged antibiotic and negatively-charge bacterial cell wall (39).

Given the polycationic nature of both spermine and aminoglycosides at physiological pH and the observed resistance of the *ktr* mutants to these otherwise unrelated molecules, we hypothesized that an alteration in cell-surface charge, coupled with altered membrane depolarization, could explain the observed change in resistance. To test this hypothesis, we measured survival of the *ktr* double mutant in polymyxin B, an unrelated polycationic antibiotic that has a +5-charge at physiological pH (40). Consistent with our hypothesis, the *ktr* double mutant survived significantly better than the ancestor in the presence of 1 mg/mL polymyxin B (Figure 3.4C).

To assess changes in bacterial cell surface charge, we measured cytochrome C binding in the ancestral MN8 and *ktr* double mutant strains (Figure 3.4D). Cytochrome C binding provides a convenient proxy to infer bacterial cell-surface charge as it is highly cationic and binds effectively to the negatively charged bacterial cell wall (41). We detected a significant increase in the percent of unbound cytochrome C in the *ktr* mutant when compared to the ancestral strain, consistent with an increase in cell surface charge conferred by *ktr* mutations (Figure 3.4D). Taken together, our findings suggest a novel mechanism by which modulation of potassium transport complex function confers resistance to diverse cationic antimicrobial compounds through changes in electrostatic properties of the bacterial cell surface.

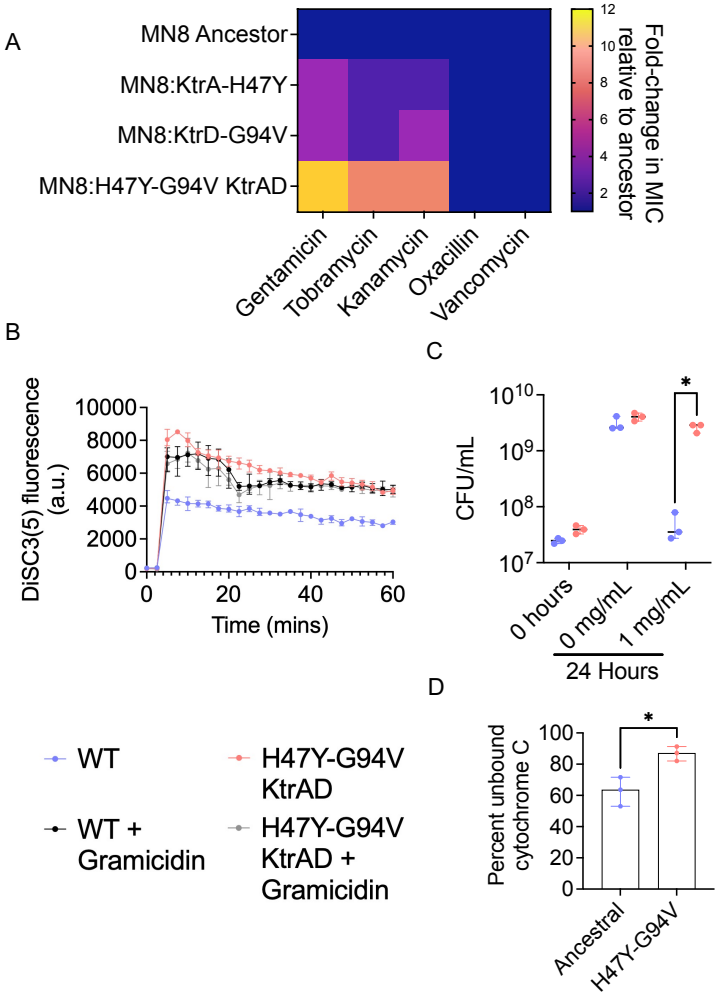

Figure 3.4 KtrAD complex mutations alter antibiotic resistance, membrane potential, and cell-surface charge.

A. Heatmap depicting fold-change in MIC for indicated antibiotics in *S. aureus* mutant strains relative to the ancestor. Values represent the average of three experiments each conducted in triplicate. **B.** 3,3'-Dipropylthiadicarbocyanine Iodide (DiSC3(5)) fluorescence of different engineered strains. Fluorescence readings are normalized to OD600 measurements for each respective strains. Points on the graph each represent average of a different experiment conducted in triplicate. **C.** CFUs of the ancestral MN8 strain or double *ktrAD* mutant measured after 24 hours of incubation with polymyxin B. Points represent average of a different experiment conducted in triplicate. Asterisks represent significant difference ($P<0.05$) in means between two groups compared as detected by an unpaired T-test. **D.** Percent unbound cytochrome C measured via absorbance at 410 nm in a spectrophotometric plate reader. Percent unbound cytochrome C was calculated relative to the absorbance of cytochrome C alone in buffer without cells. Asterisks represent significant difference ($P<0.001$) as determined by an unpaired T-test.

Exogenous potassium is insufficient to confer spermine resistance in S. aureus

Given that *ktr* mutants identified in this study exhibit opposite drug resistance phenotypes compared to published *ktr* deletion mutants (37), we hypothesized that our evolved mutants do not result in a complete loss of function. We therefore considered whether changes in exogenous potassium might reveal an effect on spermine toxicity. To test this, we generated a chemically defined medium lacking excess potassium following previously published formulations (34). This allowed us to supplement the growth medium with defined amounts of potassium in the form of KCl. We supplemented the media with physiologically relevant amounts of potassium by adding 0.1 mM and 10 mM KCl. Exogenous potassium levels had no measurable difference on the amount of CFUs recovered across different concentrations of spermine (Fig. 5). Overall, spermine appears to be slightly more toxic to the cells in this environment, however this is to be expected for a minimal media in comparison to TSB. This experiment indicates that changes in physiologically-relevant potassium levels are not sufficient to alter spermine resistance. We did observe that extremely high levels of potassium (250 mM) appeared to increase resistance to polyamines as well as aminoglycosides (Supplemental Figure S3.5). However, at these levels it is unclear whether potassium is acting functioning direction through bacterial cells, or rather by interfering with the ability of antimicrobials to interact with the bacterial cell surface. Further work will be necessary in order to more precisely determine the mechanistic basis of evolved mutations on Ktr complex functioning.

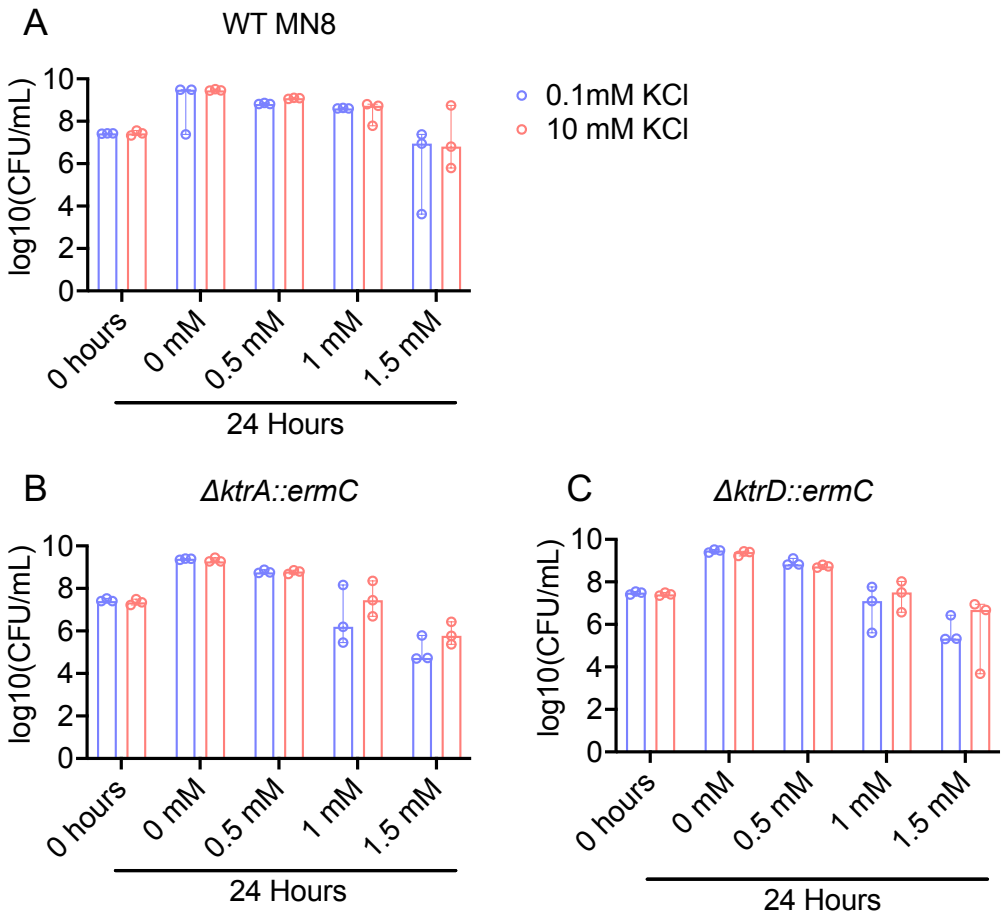

Figure 3.5: Exogenous KCl supplemented in chemically defined media does not reduce the toxic effects of spermine in *S. aureus*
Enumerations of colony forming units after 24 hours of incubations in different amounts of spermine in media with high, and low amounts of KCl for A) WT *S. aureus* MN8, B) Δ*ktrA::ermC,* or C) Δ*ktrD::ermC* strains.

Discussion

Our study identifies a previously unknown role for the Ktr potassium transport complex in *S. aureus* resistance to diverse cationic antimicrobials. A recent study also recovered mutations in *ktr* genes after passaging *S. aureus* in the presence of a synthetic polyamine, although the effects of these mutations were not reported (42). It is notable that phenotypes conferred by single amino acid changes in the Ktr complex recovered during experimental evolution are markedly different

from Δ*ktr* strains described previously (32). Evolved *ktrA* and *ktrD* mutations in this study uniformly decreased sensitivity to aminoglycoside antibiotics and spermine, suggesting a potential gain of function. Furthermore, the Δ*ktrA* and Δ*ktrD* mutants did not change the sensitivity to spermine relative to the ancestral MN8 strain (Figure 3.1). Initially, we hypothesized that the Ktr mutations resulted in increased import of potassium into the cell. However, our experiments supplementing media with KCl and growth in different KCl concentrations do not support this model (Figure 3.5, Supplemental figures S3.1-S3.3). The results in this work highlight the necessity to study Ktr-mediated potassium transport across a wider array of *S. aureus* strains. Currently, our understanding regarding the function of the Ktr system in *S. aureus* is based on work in USA300 strains only. Notably, in *S. aureus,* the Ktr complex functions as a unique combination of a single channel regulator (*ktrA)*, and multiple ion channels (*ktrB/D),* that are both regulated by *ktrA.* The unique channel architecture suggests that Ktr could provide distinct functions across *S. aureus* isolates that differ from those characterized in other bacteria. The same evolved mutations in *ktr* genes also altered membrane potential and cell-surface charge, which may contribute to spermine and aminoglycoside resistance. Links between potassium transport and membrane potential are well-documented, although there is a lack of evidence in the literature regarding the role potassium transport in regulating bacterial cell surface charge (43). Notably, a previous study also found that potassium transport can alter zeta potential (the voltage field that arises from a cell surface) in a red blood cell model (44). Work is ongoing to clarify the connections between Ktr complex function, bacterial physiology, and resistance to antimicrobial agents. Notably, the relationship between cations, polyamines, aminoglycosides, and Gram-positive bacteria has been noted previously (45). This work demonstrated that aminoglycosides, spermidine, and magnesium cations compete for binding wall-teichoic acids on Gram-positive

bacterial cell walls. Future studies could aid in further clarifying how alterations in cell envelope architecture influence susceptibility to polyamines and other cationic antimicrobials.

How independent mutations in the Ktr complex together act to enhance the resistance phenotype remains unknown. It is possible that these mutations increase the permeability or sensitivity of the transporter complex. Mutations were identified in different regions of each subunit and within the complex, suggesting there is not a single interaction interface that is being modified by these mutations. Further mechanistic studies of Ktr complex mutations and their biochemical effects could aid in resolving these questions, as well as unraveling the broader connections between potassium transport and antimicrobial resistance.

The observation that natural *S. aureus* isolates carry identical mutations in Ktr complex genes as those recovered in our experiments suggests that changes in potassium transport may confer important fitness advantages during human colonization or infection (Table S3.3). The fact that these mutations are observed repeatedly but do not appear to be fixed in major *S. aureus* lineages suggests that they have arisen *de novo* during human colonization or infection. This would be consistent with other drug resistance mutations that provide a fitness benefit under certain conditions but also carry fitness trade-offs in the absence of drug. Notably, we find that Ktr mutations provide enhanced resistance to diverse cationic antimicrobials, potentially through alterations in bacterial cell surface charge (Fig. 3.4). In *S. aureus,* changes in cell-surface charge can reduce susceptibility to both daptomycin and vancomycin, two antibiotics of choice for treating MRSA infections (46, 47). Additionally, cell surface charge alterations can promote defense against host-encoded antimicrobial peptides, suggesting a potential strategy for *S. aureus* to establish an infection in the host environment (47, 48). Despite this, mutations in the Ktr complex come at a slight fitness cost, primarily as an extended lag phase in rich media

(Supplemental figure S3.3). Further studies to understand the contribution of Ktr complex function during human infections or drug resistance could aid in addressing these questions.

Our findings illustrate how combining laboratory experimental evolution with natural strain population genomics can provide unique insights on the genetic basis of pathogen adaptation. In this study, mutations in *ktrA* and *ktrD* were detected in the MN8 strain background (Table 3.1). Conversely, mutations in *pgl,* a gene that encodes for a lactonase and acts in the pentose phosphate pathway were not recovered in MN8, frequently recovered in both HFH-30364 and RN4850 strains (Table 3.1, Supplemental tables S3.1-S3.12). Notably, mutations in *pgl* are known to affect cell-wall specific phenotypes, such as sensitivity to þ-lactam antibiotics and cell-wall permeable compounds (50, 51). In addition, *pgl* mutations increase the cell-surface charge of *S. aureus*, similar to our observations in evolved *ktr* mutants (50, 51). This data suggests the potential for convergent evolution of spermine resistance at the mechanistic level, albeit via different genetic mechanisms. Future work could investigate if strain-specific differences in cell-wall composition predispose antimicrobial resistance to evolve via mutations in either *ktr* or *pgl.* Why mutations in *ktrA* and *ktrD*, but not *ktrB*, were recovered during our experiments is unclear. This could reflect unique differences in expression or regulation of these subunits in *S. aureus* or within particular strains. Alternatively, these observations could be due to as-yet undescribed functional differences in *ktrB* and *ktrD* function within the complex. Additional work leveraging targeted mutagenesis could aid in resolving potential unique roles of these Ktr complex subunits.

While this study has identified new bacterial genes and pathways that contribute to polyamine resistance, the mechanism underlying polyamine toxicity in *S. aureus* remains mysterious. Previous efforts to characterize spermine toxicity revealed the gene *menD* as a potential target, revealing the electron carrier menadione as an important factor in mediating

toxicity (16, 52). This study found that inactivation of *menD,* the gene that encodes for a menaquinone biosynthetic protein in *S. aureus,* increased resistance to spermine under aerobic conditions. While we did not recover mutations in *menD* during experimental evolution, it is possible that inactivating *menD* similarly alters the membrane potential and cell-surface charge of *S. aureus,* indicating a similar mechanism of resistance (53, 54). Alternatively, it is possible that menadione interacts with polyamines to produce a toxic byproduct that kills *S. aureus* (16). Questions also remain regarding the mechanism of polyamine resistance provided by *speG*. While *speG* homologs are known to acetylate polyamines and acetyltransferase activity is required for *speG*-mediated polyamine resistance, it is unclear specifically how acetylation counteracts polyamine toxicity. Although acetylation partly reduces the positive charge of polyamines, they also exert stronger antimicrobial activity at high pH when their positive charge is reduced (16, 51). Ultimately, the mechanism of bacterial killing by polyamines will continue to be an important area of investigation and could additionally aid in clarifying mechanisms of evolved polyamine resistance. Together this study reveals a new role for potassium transport in the unique polyamine susceptibility of *S. aureus*, with consequences for the evolution of multidrug resistance in this major human pathogen.

References

1. Sollid JUE, Furberg AS, Hanssen AM, Johannessen M. 2014. Staphylococcus aureus: determinants of human carriage. Infect Genet Evol 21:531–541.

2. Liu W, Liu Z, Yao Z, Fan Y, Ye X, Chen S. 2015. The prevalence and influencing factors of methicillin-resistant Staphylococcus aureus carriage in people in contact with livestock: A systematic review. Am J Infect Control 43:469–475.

3. Burian M, Wolz C, Goerke C. 2010. Regulatory adaptation of Staphylococcus aureus during nasal colonization of humans. PLoS One 5:e10040.

4. Wertheim HFL, Vos MC, Ott A, van Belkum A, Voss A, Kluytmans JAJW, van Keulen PHJ, Vandenbroucke-Grauls CMJE, Meester MHM, Verbrugh HA. 2004. Risk and outcome of nosocomial Staphylococcus aureus bacteraemia in nasal carriers versus non-carriers. Lancet 364:703–705.

5. Thwaites GE, Edgeworth JD, Gkrania-Klotsas E, Kirby A, Tilley R, Török ME, Walker S, Wertheim HF, Wilson P, Llewelyn MJ, UK Clinical Infection Research Group. 2011. Clinical management of Staphylococcus aureus bacteraemia. Lancet Infect Dis 11:208–222.

6. Thomer L, Schneewind O, Missiakas D. 2016. Pathogenesis of Staphylococcus aureus Bloodstream Infections. Annu Rev Pathol 11:343–364.

7. Olson ME, Horswill AR. 2013. Staphylococcus aureus osteomyelitis: bad to the bone. Cell Host Microbe. Elsevier BV.

8. Turner NA, Sharma-Kuinkel BK, Maskarinec SA, Eichenberger EM, Shah PP, Carugati M, Holland TL, Fowler VG Jr. 2019. Methicillin-resistant Staphylococcus aureus: an overview of basic and clinical research. Nat Rev Microbiol 17:203–218.

9. McAdam PR, Templeton KE, Edwards GF, Holden MTG, Feil EJ, Aanensen DM, Bargawi HJA, Spratt BG, Bentley SD, Parkhill J, Enright MC, Holmes A, Girvan EK, Godfrey PA, Feldgarden M, Kearns AM, Rambaut A, Robinson DA, Fitzgerald JR. 2012. Molecular tracing of the emergence, adaptation, and transmission of hospital-associated methicillin-resistant Staphylococcus aureus. Proc Natl Acad Sci U S A 109:9107–9112.

10. GBD 2019 Antimicrobial Resistance Collaborators. 2022. Global mortality associated with 33 bacterial pathogens in 2019: a systematic analysis for the Global Burden of Disease Study 2019. Lancet 400:2221–2248.

11. Antimicrobial Resistance Collaborators. 2022. Global burden of bacterial antimicrobial resistance in 2019: a systematic analysis. Lancet 399:629–655.

12. Parlet CP, Brown MM, Horswill AR. 2019. Commensal staphylococci influence Staphylococcus aureus skin colonization and disease. Trends Microbiol 27:497–507.

13. Howden BP, Giulieri SG, Wong Fok Lung T, Baines SL, Sharkey LK, Lee JYH, Hachani A, Monk IR, Stinear TP. 2023. Staphylococcus aureus host interactions and adaptation. Nat Rev Microbiol 21:380–395.

14. Ledger EVK, Mesnage S, Edwards AM. 2022. Human serum triggers antibiotic tolerance in Staphylococcus aureus. Nat Commun 13:2041.

15. Lehman MK, Sturd NA, Razvi F, Wellems DL, Carson SD, Fey PD. 2023. Proline transporters ProT and PutP are required for Staphylococcus aureus infection. PLoS Pathog

16. Joshi GS, Spontak JS, Klapper DG, Richardson AR. 2011. Arginine catabolic mobile element encoded speG abrogates the unique hypersensitivity of Staphylococcus aureus to exogenous polyamines. Mol Microbiol 82:9–20.

17. Thurlow LR, Joshi GS, Richardson AR. 2012. Virulence strategies of the dominant USA300 lineage of community-associated methicillin-resistant Staphylococcus aureus (CA-MRSA). FEMS Immunol Med Microbiol 65:5–22.

18. Michael AJ. 2016. Polyamines in eukaryotes, bacteria, and Archaea. J Biol Chem 291:14896–14903.

19. Igarashi K, Kashiwagi K. 2010. Modulation of cellular function by polyamines. Int J Biochem Cell Biol 42:39–51.

20. Michael AJ. 2016. Biosynthesis of polyamines and polyamine-containing molecules. Biochem J 473:2315–2329.

21. Minguet EG, Vera-Sirera F, Marina A, Carbonell J, Blázquez MA. 2008. Evolutionary diversification in polyamine biosynthesis. Mol Biol Evol 25:2119–2128.

22. Chattopadhyay MK, Tabor CW, Tabor H. 2002. Absolute requirement of spermidine for growth and cell cycle progression of fission yeast (Schizosaccharomyces pombe). Proc Natl Acad Sci U S A 99:10330–10334.

23. Imai A, Matsuyama T, Hanzawa Y, Akiyama T, Tamaoki M, Saji H, Shirano Y, Kato T, Hayashi H, Shibata D, Tabata S, Komeda Y, Takahashi T. 2004. Spermidine synthase genes are essential for survival of Arabidopsis. Plant Physiol 135:1565–1573.

24. Bae D-H, Lane DJR, Jansson PJ, Richardson DR. 2018. The old and new biochemistry of polyamines. Biochim Biophys Acta Gen Subj 1862:2053–2068.

25. Wallace HM, Fraser AV, Hughes A. 2003. A perspective of polyamine metabolism. Biochem J 376:1–14.

26. Tabor CW, Tabor H. 1985. Polyamines in microorganisms. Microbiol Rev 49:81–99.

27. Shah P, Swiatlo E. 2008. A multifaceted role for polyamines in bacterial pathogens. Mol Microbiol 68:4–16.

28. Thurlow LR, Joshi GS, Clark JR, Spontak JS, Neely CJ, Maile R, Richardson AR. 2013. Functional Modularity of the Arginine Catabolic Mobile Element Contributes to the Success of USA300 Methicillin-Resistant Staphylococcus aureus. Cell Host Microbe 13:100–107.

29. Planet PJ, LaRussa SJ, Dana A, Smith H, Xu A, Ryan C, Uhlemann A-C, Boundy S, Goldberg J, Narechania A, Kulkarni R, Ratner AJ, Geoghegan JA, Kolokotronis S-O, Prince A. 2013. Emergence of the epidemic methicillin-resistant Staphylococcus aureus strain USA300 coincides with horizontal transfer of the arginine catabolic mobile element and speG-mediated adaptations for survival on skin. MBio 4:e00889-13.

30. Diep BA, Gill SR, Chang RF, Phan TH, Chen JH, Davidson MG, Lin F, Lin J, Carleton HA, Mongodin EF, Sensabaugh GF, Perdreau-Remington F. 2006. Complete genome sequence of USA300, an epidemic clone of community-acquired meticillin-resistant Staphylococcus aureus. Lancet 367:731–739.

31. Planet PJ, Diaz L, Kolokotronis S-O, Narechania A, Reyes J, Xing G, Rincon S, Smith H, Panesso D, Ryan C, Smith DP, Guzman M, Zurita J, Sebra R, Deikus G, Nolan RL, Tenover FC, Weinstock GM, Robinson DA, Arias CA. 2015. Parallel epidemics of community-associated methicillin-resistant Staphylococcus aureus USA300 infection in north and South America. J Infect Dis 212:1874–1882.

32. Gries CM, Bose JL, Nuxoll AS, Fey PD, Bayles KW. 2013. The Ktr potassium transport system in Staphylococcus aureus and its role in cell physiology, antimicrobial resistance and pathogenesis. Mol Microbiol 89:760–773.

33. Gries CM, Sadykov MR, Bulock LL, Chaudhari SS, Thomas VC, Bose JL, Bayles KW. 2016. Potassium Uptake Modulates Staphylococcus aureus Metabolism. mSphere 1.

34. Price-Whelan A, Poon CK, Benson MA, Eidem TT, Roux CM, Boyd JM, Dunman PM, Torres VJ, Krulwich TA. 2013. Transcriptional profiling of Staphylococcus aureus during growth in 2 M NaCl leads to clarification of physiological roles for Kdp and Ktr K+ uptake systems. MBio 4.

35. Radlinski LC, Rowe SE, Brzozowski R, Wilkinson AD, Huang R, Eswara P, Conlon BP. 2019. Chemical induction of aminoglycoside uptake overcomes antibiotic tolerance and resistance in Staphylococcus aureus. Cell Chem Biol 26:1355-1364.e4.

36. Farha MA, Verschoor CP, Bowdish D, Brown ED. 2013. Collapsing the proton motive force to identify synergistic combinations against Staphylococcus aureus. Chem Biol 20:1168–1178.

37. Bakker EP, Mangerich WE. 1981. Interconversion of components of the bacterial proton motive force by electrogenic potassium transport. J Bacteriol 147:820–826.

38 .Epstein W. 2003. The roles and regulation of potassium in bacteria. Prog Nucleic Acid Res Mol Biol 75:293–320.

39. Serio AW, Keepers T, Andrews L, Krause KM. 2018. Aminoglycoside revival: Review of a historically important class of antimicrobials undergoing rejuvenation. EcoSal Plus 8.

40. Vaara M, Fox J, Loidl G, Siikanen O, Apajalahti J, Hansen F, Frimodt-Møller N, Nagai J, Takano M, Vaara T. 2008. Novel polymyxin derivatives carrying only three positive charges are effective antibacterial agents. Antimicrob Agents Chemother 52:3229–3236.

41. Nikolic P, Mudgil P, Harman DG, Whitehall J. 2022. Untargeted lipidomic differences between clinical strains of methicillin-sensitive and methicillin-resistant Staphylococcus aureus. Infect Dis (Lond) 54:497–507.

42. Douglas EJA, Alkhzem AH, Wonfor T, Li S, Woodman TJ, Blagbrough IS, Laabei M. 2022. Antibacterial activity of novel linear polyamines against Staphylococcus aureus. Front Microbiol 13:948343.

43. Benarroch JM, Asally M. 2020. The microbiologist's guide to membrane potential dynamics. Trends Microbiol 28:304–314.

44. Hughes MP, Fry CH, Labeed FH. 2022. Cytoplasmic anion/cation imbalances applied across the membrane capacitance may form a significant component of the resting membrane potential of red blood cells. Sci Rep 12:15005.

45. Rozansky R, Bachrach U, Grossowicz N. 1954. Studies on the antibacterial action of spermine. J Gen Microbiol 10:11–16.

46. Jones T, Yeaman MR, Sakoulas G, Yang S-J, Proctor RA, Sahl H-G, Schrenzel J, Xiong YQ, Bayer AS. 2008. Failures in clinical treatment of Staphylococcus aureus Infection with daptomycin are associated with alterations in surface charge, membrane phospholipid asymmetry, and drug binding. Antimicrob Agents Chemother 52:269–278.

47. Ernst CM, Slavetinsky CJ, Kuhn S, Hauser JN, Nega M, Mishra NN, Gekeler C, Bayer AS, Peschel A. 2018. Gain-of-function mutations in the phospholipid flippase MprF confer specific daptomycin resistance. MBio 9.

48. Joo H-S, Otto M. 2015. Mechanisms of resistance to antimicrobial peptides in staphylococci. Biochim Biophys Acta Biomembr 1848:3055–3061.

49. J, Kim GL, Norambuena J, Boyd JM, Parker D. 2023 Impact of the pentose phosphate pathway on metabolism and pathogenesis of Staphylococcus aureus. PLOS Pathogens 19(7): e1011531

50. Zeden MS, Gallagher LA, Bueno E, Nolan AC, Ahn J, et al. 2023 Metabolic reprogramming and altered cell envelope characteristics in a pentose phosphate pathway mutant increases MRSA resistance to β-lactam antibiotics. PLOS Pathogens 19(7): e1011536

51. Anzaldi LL, Skaar EP. 2011. The evolution of a superbug: how Staphylococcus aureus overcomes its unique susceptibility to polyamines. Mol Microbiol.

52. von Eiff C, McNamara P, Becker K, Bates D, Lei X-H, Ziman M, Bochner BR, Peters G, Proctor RA. 2006. Phenotype microarray profiling of Staphylococcus aureus menD and hemB mutants with the small-colony-variant phenotype. J Bacteriol 188:687–693

53. Hammer ND, Reniere ML, Cassat JE, Zhang Y, Hirsch AO, Indriati Hood M, Skaar EP. 2013. Two Heme-Dependent Terminal Oxidases Power Staphylococcus aureus Organ-Specific Colonization of the Vertebrate Host. MBio 4:e00241-13-e00241-13.

54. Deatherage, D.E., Barrick, J.E. 2014. Identification of Mutations in Laboratory-Evolved Microbes from Next-Generation Sequencing Data Using *breseq* . In: Sun, L., Shou, W. (eds) Engineering and Analyzing Multicellular Systems. Methods in Molecular Biology, vol 1151. Humana Press, New York, NY.

55. Monk I, Shah I, Xu, M, Tan M. 2012 Transforming the Untransformable: Application of Direct Transformation To Manipulate Genetically Staphylococcus aureus and Staphylococcus epidermidis. MBio. *3*(2), 10-1128

56. Löfblom J, Kronqvist N, Uhlén M, Ståhl S, Wernérus H. 2007. Optimization of electroporation-mediated transformation: Staphylococcus carnosus as model organism. J Appl Microbiol

57. Zheng X, Marsman G, Lacey KA, Chapman JR, Goosmann C, Ueberheide BM, Torres VJ. 2021. The cell envelope of Staphylococcus aureus selectively controls the sorting of virulence factors. Nat Commun 12:6193.

58. Te Winkel, J. D., Gray, D. A., Seistrup, K. H., Hamoen, L. W., & Strahl, H. 2016. Analysis of antimicrobial-triggered membrane depolarization using voltage sensitive dyes. Frontiers in cell and developmental biology, *4*, 29

CHAPTER IV
UNRAVELING OTHER ROLES FOR KTR-MEDIATED POTASSIUM TRANSPORT IN S. AUREUS

All data in this chapter is unpublished. This chapter arose as a series of conversations between myself and Matt Barber and is a follow-up the published work from Chapter III.

Introduction

To date, studies thoroughly investigating the full spectrum of potassium transport system functions in *S. aureus* are lacking. This is surprising given that potassium is the most abundant intracellular cation inside bacterial cells (1). Despite this, extracellular concentrations of potassium are often limited (1, 2), presenting a conundrum for the bacterial cell: acquiring potassium against steep concentration gradients. Furthermore, potassium transport is known to mediate a variety of basic cellular processes and stress responses in *S.* aureus, including regulation of protein synthesis, adjusting membrane potential, managing alkaline stress, maintaining intracellular pH, maintaining turgor pressure, and potentially mediating stress from osmotic shock (1). Because potassium transport underpins so many fundamental cellular processes, bacteria have evolved multiple mechanisms for acquiring potassium. To date, four different potassium transport systems have been identified in bacteria: Trk, Ktr, Kdp and Kup (3, 4). Each transport system contains an ion conducting protein that is part of the conserved Superfamily of K+ transporters (SKT)(3-7). As previously mentioned in Chapter III, two potassium transport systems have been identified in *S. aureus:* Ktr, and Kdp (8, 9). The Ktr

system is comprised of three different proteins, KtrA, KtrB, and KtrD. Both KtrB and KtrD assemble as transmembrane homodimers, while KtrA is an octameric protein complex that exists on the cytoplasmic side of the bacterial cell membrane (8, 9). KtrA together with KtrB or KtrD forms the entire Ktr potassium transport system of *S. aureus* (8, 9). Interestingly, the Ktr architecture found in *S. aureus* is unique, as Ktr systems found in other bacterial species typically are composed of two ion conducting subunits (KtrB or KtrD) that each pair with a specific regulatory subunit (KtrA or KtrC). (10, 11) The exact role of the unique *S. aureus* Ktr architecture remains a mystery, but it opens the possibility that *S. aureus* Ktr may influence cellular processes beyond what is typically thought to be relevant for potassium transporters.

Previous work has noted the unique architecture of the Ktr complex, and confirmed its important role in potassium acquisition (9). This work also revealed that the Ktr complex is essential in alkaline conditions that also are extremely potassium limited (9). Moreover, these authors identified a role for the Ktr system in tolerating various stressors. For example, the authors noted that deleting the *ktr* genes resulted in uniformly more sensitivity to antibiotics and host-encoded antimicrobial peptides (9). This same study determined that the Ktr system is important for survival in a mouse bacteremia model (9), indicating that modulation of potassium transport may be a strategy for the cell to survive stressors encountered in the host environment. My own work reified these findings through the discovery that mutations in *ktr* genes conferred increased capacity to survive antimicrobial stress from polyamines as well as other antibiotics (12). These findings were further reinforced when I discovered that the same Ktr mutations recovered in our evolution experiment are present in various published genome sequences of *S. aureus* isolates, indicating a potential role for alteration of Ktr function to be an adaptive solution in response to various pressures. However, how the mutations I recovered mechanistically affect

the basic functioning of the Ktr complex, and how that, in turn, changes tolerance of host-encoded pressures remains unknown.

In this chapter, I will present preliminary results from my efforts to further identify the mechanistic alterations to Ktr function encoded by the mutations discovered in the previous evolution experiment. I then present a set of experiments that will further elucidate the roles of Ktr-mediated potassium transport in tolerating host-encoded stressors.

Results

To determine the baseline functionality of the Ktr system in *S. aureus,* I first performed growth assays under conditions that are known to require normal Ktr function. By doing this, I could determine if the mutations recovered in the evolution experiment in Chapter III are gain-of-function, loss-of-function, or altering the function in some other way. To do this, I leveraged strains I had engineered previously in Chapter III. Briefly, those are: Wild-type (WT) *S. aureus* MN8, *S. aureus* MN8 Δ*ktrA::ermC* (*S. aureus* MN8 lacking a functional Ktr system), and *S. aureus* H47Y-G94V KtrAD (*S. aureus* MN8 with two single amino acid changes engineered into the ancestral Ktr loci). I grew these strains under varying pH and potassium levels in a semi-defined media and measured their growth continuously for 20 hours. I discovered that the Ktr double mutant and the Ktr-null strains grow comparably to WT at neutral pH and potassium-limited conditions (Figure 4.1A,B). However, as I increased the potassium and alkalinity of the media, I noticed a discernable growth defect in the Ktr double mutant (Figure 4.1C,D). The most obvious growth deficiency occurred when I supplemented the media with 10 mM of potassium chloride (KCl) and adjusted the pH to 8.7 (Figure 4.1D). Interestingly, the Ktr double mutant experienced unique changes in metabolism as demonstrated by the presence of multiple, diauxic

shifts in the growth curves at pH 8.7 (Figure 4.1C,D). Diauxic shifts typically occur when bacterial cells are switching from metabolizing one carbon source to another, demonstrated by an initial logarithmic growth phase, followed by a lag phase, then a second logarithmic growth phase (17). While all genotypes experienced a visible diauxic shift, the Ktr double mutant experienced the longest lag phases during growth, indicating an impaired ability to metabolize available carbon sources. This observation is consistent with the important role for potassium acquisition in maintaining the electrochemical gradient across the cell membrane (13-15). This partition of charges also establishes the proton motive force (PMF) which, in turn is responsible for driving the synthesis of ATP via oxidative phosphorylation (17, 18). Therefore, it is reasonable to hypothesize that perturbing the electrochemical gradient by altering potassium ion acquisition may impair the Ktr double mutant's ability to generate ATP.

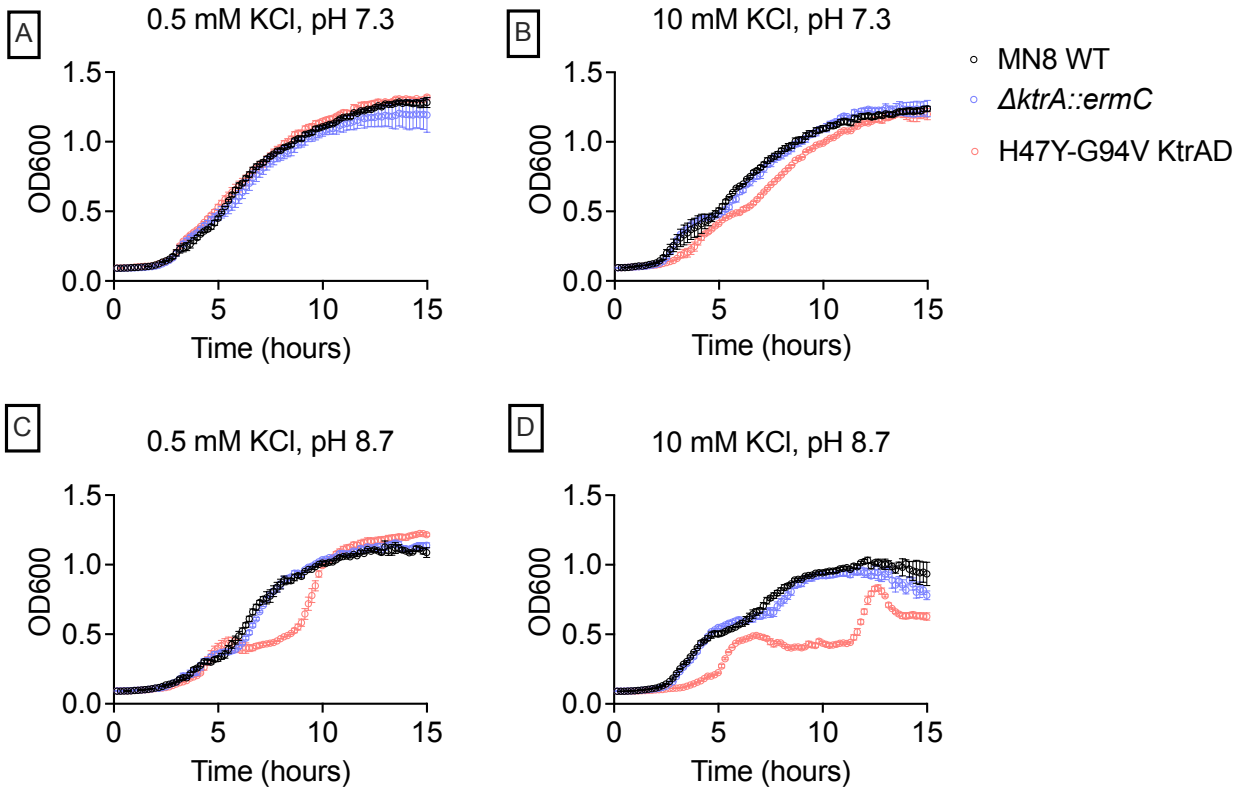

Figure 4.1: Ktr double mutants exhibit growth defects at elevated pH and potassium. Different genotypes of *S. aureus* MN8 grown in chemically-defined medium containing 0.5 mM KCl (Panels A,C) or 10 mM of KCl (Panels B,D) at neutral pH (Panels A,B) or alkaline pH.(panels C,D). Optical density (OD600) measurements taken every 10 minutes for 15 hours.

After obtaining these initial results, I sought to understand if adding extremely high amounts of potassium to the media could exacerbate the differences in growth observed in Figure 4.1. Indeed, when increasing the concentration of potassium in the media, I observed a larger defect in growth between the Ktr double mutant and the WT strain (Figure 4.2). This growth defect was illustrated by a prolonged lag phase in the growth curve of the KtrAD double mutant under alkaline conditions (Figure 4.2B).

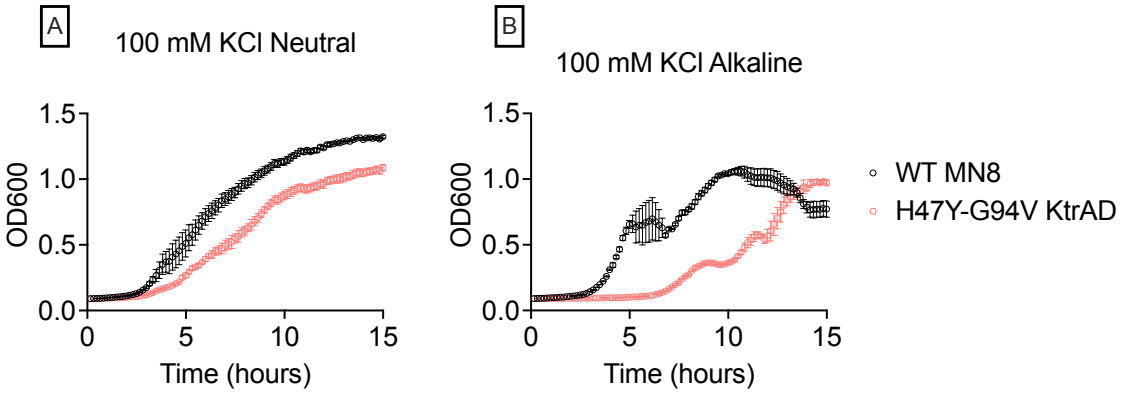

Figure 4.2: Extremely elevated KCl levels result in Ktr double mutant growth deficiency
Growth curves conducted for both WT *S. aureus* MN8 and the H47Y-G94V KtrAD genotypes. OD600 measured every 10 minutes for 15 hours.

Given that higher levels of potassium and pH are causing an extended lag phase in Ktr mutants, I sought to understand what physiological process might be driving this phenotype. Previously I found that the KtrAD double mutant has a relatively depolarized membrane in comparison to the *S. aureus* MN8 WT (Figure 3.4B). Depolarization of the bacterial membrane is typically deleterious for the cell, and is often a toxic consequence of antibacterial peptides (19-21). Therefore, it was curious that the fittest genotype recovered from the evolution experiment had an extremely depolarized membrane relative to the WT. This paradox was further compounded by the fact that maintaining these mutations in the Ktr complex seemed to pose a fitness disadvantage as demonstrated by their poor growth under various conditions (Figures 4.1, 4.2, Supplemental Figure S3.1-S3.3). As result, I wondered if the selection environment resulted in cells becoming hyperpolarized—an equally deleterious, but opposite effect of depolarization (22). I hypothesized that the KtrAD double mutant had evolved to maintain a depolarized membrane because the selection environment created hyperpolarized membranes in the cells, and

individual cells that harbored mutations that resulted in depolarized membranes were able to better survive. To test this, I conducted the same membrane potential assay as previously shown in Chapter III, however this time I measured the membrane potential of the cells with spermine added to the media at the same concentration that I began the selection experiment with (2mM). I observed that adding spermine to the environment resulted in a small, but appreciable hyperpolarization of the cell membranes, consistent with my hypothesis. (Figure 4.3).

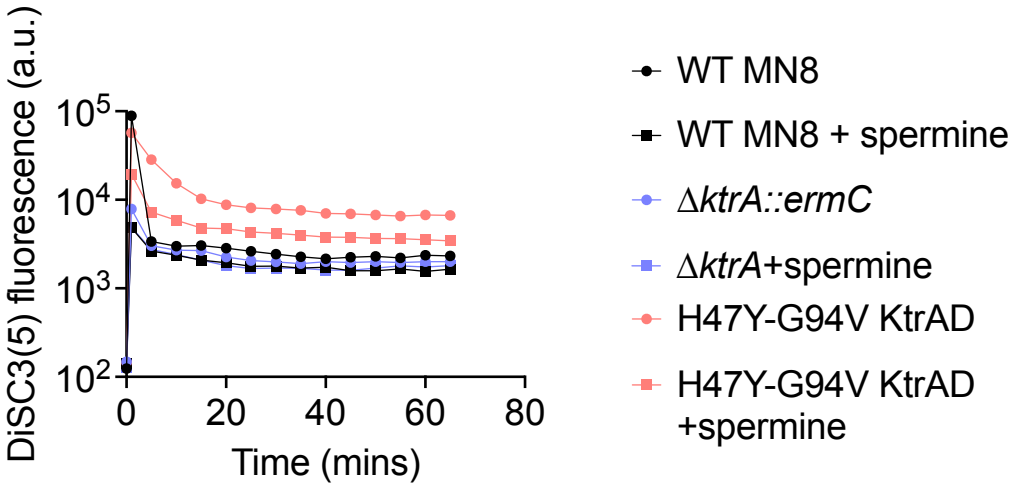

Figure 4.3: Membrane potential measurements with spermine present
3,3'-Dipropylthiadicarbocyanine Iodide (DiSC3(5)) fluorescence of different engineered strains. Fluorescence readings are normalized to OD600 measurements for each respective strains. Points on the graph each represent average of a different experiment conducted in triplicate

Proposed Experiments Currently in Progress

While my published work as identified new roles for potassium transporters in antimicrobial resistance, many questions remain to be addressed. For example, it is unclear how evolved mutations are impacting Ktr complex function and cell physiology. Bacterial membranes become depolarized when the electrochemical difference from the inside of the membrane relative to the outside becomes more positive (15, 23). This can be influenced by a variety of factors, including potassium transport (11). Specifically, excessive intracellular potassium levels

can depolarize cell membranes. Therefore, I hypothesize that evolved mutations in the Ktr complex (H47Y-G94V KtrAD) are leading to constitutive potassium import. In this unregulated state, *S. aureus* cells cannot control the amounts of potassium inside the cell and thus are more susceptible to extracellular concentrations of potassium in the environment. In this scenario, I hypothesize that higher amounts of potassium in the environment would result in higher intracellular levels of potassium in the Ktr double mutants relative to WT cells. This would contribute to depolarizing the membrane by reducing the difference in charge across the bacterial membrane. I hypothesize that this change in membrane potential would also result in decreased ATP, as the loss of membrane potential would also impair the proton motive force required for powering ATP production. This hypothesis is consistent with initial results measuring the membrane polarity of Ktr double mutants, as well as the elongated lag phases shown in the growth curves under alkaline pH and high KCl concentrations (Figures 3.4, 4.1-4.3). To more directly test the hypotheses above, I propose the following experiments.

Inductively Coupled Plasma Mass Spectrometry to Determine Intracellular Concentrations of Potassium

Inductively coupled plasma mass spectrometry (ICP-MS) is an analytical chemistry technique that can be used to measure elements present in a biological sample (24). I intend to leverage this technique to measure intracellular amounts of potassium across a panel of *S. aureus* genotypes. By doing this, I can determine if the mutations I identified in *ktr* genes are imparting gain-of-function or loss-of-function phenotypes. If the mutations are gain-of-function, I hypothesize that the Ktr-double mutant should import more potassium ions into the cell relative to the wild-type. I will measure this by preparing overnight cultures of *S. aureus* MN8 WT, *S.*

aureus H47Y-G94V KtrAD, and *S. aureus* Δ*ktrA::ermC,* in semi-defined media with 10mM of potassium-chloride (KCl). After 20 hours of growth, I will normalize the OD600 of the cultures to approximately 1.0, and wash the cultures with phosphate-buffered-saline (PBS). After this I will pellet the cells and remove all excess PBS. I will then dry the pellets and measure the dry weight of the cell pellets. The dried cell pellets will be sent to the elemental analysis core at Oregon Health Sciences University (OHSU) where the ICP-MS procedure will be performed. By doing this experiment, I will be able to directly measure how Ktr complex mutations impact cellular potassium levels.

Measuring ATP Production

Given the visual differences observed in the growth curve assays conducted under various pH levels and KCl concentrations, I want to know how mutations in the Ktr complex affect the ability of *S. aureus* to generate ATP. Previously, studies have shown that limiting the amount of potassium available to *S. aureus* can impair ATP production. However, it is not known how Ktr mutations might change the ability of *S. aureus* to generate ATP, especially if the mutations may increase the amount of intracellular potassium. I propose to measure ATP levels produced by different genotypes of *S. aureus* under a suite of different conditions. To do this, I will use the BacTiter-Glo kit (Promega) according to manufacturer instructions. This kit leverages a recombinant firefly luciferase that, in the presence of ATP from the lysed bacterial cells, reacts to emit luminescence detectable by a plate reader. I plan to measure ATP levels across the same three *S. aureus* genotypes mentioned earlier: WT MN8, Δ*ktrA::ermC,* and H47Y-G94V KtrAD. I will grow the strains under the same potassium levels and alkalinity levels as the experiments displayed in Figure 4.1. I hypothesize that the KtrAD double mutant

will have lower overall amounts of ATP production at higher potassium levels and pH, concomitant to the impaired growth they display under those conditions (Figures 4.1, 4.2).

Measuring electron transport chain function

A crucial component of Ktr function is regulating the cell's proton motive force. Proton motive force is an electrochemical gradient across the bacterial membrane established by the pumping of hydrogen ions out of the cell to then drive the synthesis of ATP (17,18). The maintenance of the proton motive force is a dynamic process that is composed of the transmembrane proton gradient (ΔpH) and the electric potential (ΔΨ) (15). Perturbations in one of these processes is compensated for by altering the other. Given that potassium ions are charged particles, transporting them across the cell membrane results in alterations to the ΔΨ. Therefore, altering Ktr function in a way that changes the electrical potential can result in alterations to the proton motive force, affecting cellular respiration and potentially ATP synthesis. I will directly measure electron transport chain activity by incubating *S. aureus* cells with the fluorescent redox dye 5-cyano-2,3-ditolyl tetrazolium chloride (CTC). CTC can accept electrons from the electron transport chain and is reduced to an insoluble, formazan, red fluorescent product, allowing me to detect the relative levels of electron transport occurring inside the *S. aureus* electron transport chain (25). To conduct this assay, I will incubate the same *S. aureus* genotypes with CTC under the same conditions as previously defined. I will then use flow-cytometry to sort the cells based on the presence or absence of red fluorescence in the cell populations, allowing me to quantify the fraction of cells in the populations have functioning electron transport chains. I hypothesize that the KtrAD double mutants will have a lower proportion of the population with a functioning electron transport chain, and that this will be

particularly apparent at elevated pH and potassium levels. This data together with the ATP quantification assay will allow me to generate a full picture of the metabolic capacity of the H47Y-G94V KtrAD mutants.

Monitoring Intracellular pH

As previously mentioned, the maintenance of the ΔpH is an important part of establishing and maintaining the proton motive force in populations of respiring cells. Therefore, I also propose to monitor the intracellular pH of *S. aureus* cells grown under the same conditions defined above. To do this, I will transform *S. aureus* cells with a plasmid encoding a pH-sensitive, yellow-fluorescent protein (YFP). As the cells are growing, fluorescence intensity can be measured and intracellular pH can be approximately calculated based on a standard curve. Following previous hypotheses, I hypothesize that the intracellular pH of the KtrAD double mutant cells will be more alkaline relative to WT. This hypothesis is based primarily on published data, indicating that Ktr-mediated import of potassium is coupled with H+ extrusion (25). Therefore, if these mutations result in elevated potassium import, I expect that elevated H+ extrusion will follow.

Global RNA-Sequencing of *S. aureus* Populations

Ktr-mediated potassium transport has been linked to changes in antimicrobial susceptibility and virulence in the host environment (11,12, 25). In my previous work, I determined that the KtrAD double mutant resulted in increased survival in the presence of cationic antibiotics (13). Given the ability for Ktr-mediated potassium transport to affect diverse phenotypes related to virulence and antimicrobial resistance, I am curious to know if and how

global gene expression patterns are affected by mutations in the Ktr potassium transport complex. To determine this, I will grow the three genotypes of *S. aureus* previously mentioned, in low (0.1mM), and high (10mM) KCl concentrations. I will then extract RNA using the RNeasy Kit (Qiagen) according to the manufacturer's instructions. I will quantify RNA quality and concentration, then send isolated RNA for sequencing to SeqCenter. *A priori*, it is difficult to predict which genes may be differentially regulated, as published work investigating changes in gene expression due to altered potassium transport are lacking. However, given the clear resistance to cationic antimicrobials conferred by these mutations, I expect that genes which increase the surface charge of the cell are upregulated in the KtrAD double mutants. Furthermore, if the KtrAD double mutant imports more potassium into the cell relative to WT, I predict that the Kdp potassium transport system is downregulated as a result.

Conclusion

In this chapter, I presented preliminary data investigating the mechanistic consequences of harboring mutations the KtrAD potassium transport complex. I also proposed hypotheses regarding why membrane depolarization might evolve as an adaptive trait within the environment of the evolution experiment, and present data to partially support that claim. I also present a series of experiments that will better define the functional capacity of the Ktr potassium transport system, and how potential gain-of-function mutations may reveal novel phenotypes in *S. aureus* not previously known. Collectively, the proposed experiments in this chapter will provide information necessary to define the mechanistic change to the KtrAD potassium transport complex conferred by the mutations I identified. Furthermore, the proposed experiments will reveal which cellular processes are affected by the mutations in the Ktr

complex. Ultimately, the data generated from these experiments will help explain the unique organization of the Staphylococcal Ktr potassium transport complex.

References

1. Bakker, E.P. and Mangerich, W.E., 1981. Interconversion of components of the bacterial proton motive force by electrogenic potassium transport. *Journal of bacteriology*, *147*(3), pp.820-826.
2. Booth, Ian R. "Regulation of cytoplasmic pH in bacteria." *Microbiological reviews* 49, no. 4 (1985): 359-378.
3. Epstein, W., 1986. Osmoregulation by potassium transport in Escherichia coli. *FEMS Microbiology Reviews*, *2*(1-2), pp.73-78.
4. Epstein, W., 2003. The roles and regulation of potassium in bacteria. *Progress in nucleic acid research and molecular biology*, *75*, pp.293-320.Doyle, D.A., Cabral, J.M., Pfuetzner, R.A., Kuo, A., Gulbis, J.M., Cohen, S.L., Chait, B.T. and MacKinnon, R., 1998. The structure of the potassium channel: molecular basis of K+ conduction and selectivity. *science*, *280*(5360), pp.69-77.
5. Doyle, D.A., Cabral, J.M., Pfuetzner, R.A., Kuo, A., Gulbis, J.M., Cohen, S.L., Chait, B.T. and MacKinnon, R., 1998. The structure of the potassium channel: molecular basis of K+ conduction and selectivity. *science*, *280*(5360), pp.69-77.
6. Roosild, T.P., Castronovo, S., Miller, S., Li, C., Rasmussen, T., Bartlett, W., Gunasekera, B., Choe, S. and Booth, I.R., 2009. KTN (RCK) domains regulate K+ channels and transporters by controlling the dimer-hinge conformation. *Structure*, *17*(6), pp.893-903.
7. Albright, R.A., Ibar, J.L.V., Kim, C.U., Gruner, S.M. and Morais-Cabral, J.H., 2006. The RCK domain of the KtrAB K+ transporter: multiple conformations of an octameric ring. *Cell*, *126*(6), pp.1147-1159.

8. Corrigan, R.M., Campeotto, I., Jeganathan, T., Roelofs, K.G., Lee, V.T. and Gründling, A., 2013. Systematic identification of conserved bacterial c-di-AMP receptor proteins. *Proceedings of the National Academy of Sciences*, *110*(22), pp.9084-9089.

9. Gries, C.M., Bose, J.L., Nuxoll, A.S., Fey, P.D. and Bayles, K.W., 2013. The Ktr potassium transport system in Staphylococcus aureus and its role in cell physiology, antimicrobial resistance and pathogenesis. *Molecular microbiology*, *89*(4), pp.760-773.

10. Vieira-Pires, R., Szollosi, A. and Morais-Cabral, J., 2013. The structure of the KtrAB potassium transporter. *Biophysical Journal*, *104*(2), p.23a.

11. Gries, C.M., Sadykov, M.R., Bulock, L.L., Chaudhari, S.S., Thomas, V.C., Bose, J.L. and Bayles, K.W., 2016. Potassium uptake modulates Staphylococcus aureus metabolism. *Msphere*, *1*(3), pp.10-1128.

12. Campbell, K., Kowalski, C.H., Kohler, K.M., Kebret, M.R. and Barber, M.F., 2025. Evolution of polyamine resistance in Staphylococcus aureus through modulation of potassium transport. *mSphere*, pp.e00613-24.

13. Price-Whelan, A., Poon, C.K., Benson, M.A., Eidem, T.T., Roux, C.M., Boyd, J.M., Dunman, P.M., Torres, V.J. and Krulwich, T.A., 2013. Transcriptional profiling of Staphylococcus aureus during growth in 2 M NaCl leads to clarification of physiological roles for Kdp and Ktr K+ uptake systems. *MBio*, *4*(4), pp.10-1128.

14. Kashket, E.R. and Barker, S.L., 1977. Effects of potassium ions on the electrical and pH gradients across the membrane of Streptococcus lactis cells. *Journal of bacteriology*, *130*(3), pp.1017-1023.

15. Benarroch, J.M. and Asally, M., 2020. The microbiologist's guide to membrane potential dynamics. *Trends in microbiology*, *28*(4), pp.304-314.

16. Salvy, P. and Hatzimanikatis, V., 2021. Emergence of diauxie as an optimal growth strategy under resource allocation constraints in cellular metabolism. *Proceedings of the National Academy of Sciences*, *118*(8), p.e2013836118.

17. Maloney, P.C., Kashket, E.R. and Wilson, T.H., 1974. A protonmotive force drives ATP synthesis in bacteria. *Proceedings of the National Academy of Sciences*, *71*(10), pp.3896-3900.

18. Fischer, S., Gräber, P. and Turina, P., 2000. The activity of the ATP synthase from Escherichia coli is regulated by the transmembrane proton motive force. *Journal of Biological Chemistry*, *275*(39), pp.30157-30162.

19. Epand, R.F., Pollard, J.E., Wright, J.O., Savage, P.B. and Epand, R.M., 2010. Depolarization, bacterial membrane composition, and the antimicrobial action of ceragenins. *Antimicrobial agents and chemotherapy*, *54*(9), pp.3708-3713.

20. Nicolas, P., 2009. Multifunctional host defense peptides: intracellular-targeting antimicrobial peptides. *The FEBS journal*, *276*(22), pp.6483-6496.

21. Wenzel, M., Chiriac, A.I., Otto, A., Zweytick, D., May, C., Schumacher, C., Gust, R., Albada, H.B., Penkova, M., Krämer, U. and Erdmann, R., 2014. Small cationic antimicrobial peptides delocalize peripheral membrane proteins. *Proceedings of the National Academy of Sciences*, *111*(14), pp.E1409-E1418.

22. Bhaumik, K.N., Spohn, R., Dunai, A., Daruka, L., Olajos, G., Zákány, F., Hetényi, A., Pál, C. and Martinek, T.A., 2024. Chemically diverse antimicrobial peptides induce hyperpolarization of the E. coli membrane. *Communications Biology*, *7*(1), p.1264.

23. Te Winkel, J.D., Gray, D.A., Seistrup, K.H., Hamoen, L.W. and Strahl, H., 2016. Analysis of antimicrobial-triggered membrane depolarization using voltage sensitive dyes. *Frontiers in cell and developmental biology*, *4*, p.29.

24. Van Acker, T., Theiner, S., Bolea-Fernandez, E., Vanhaecke, F. and Koellensperger, G., 2023. Inductively coupled plasma mass spectrometry. *Nature Reviews Methods Primers*, *3*(1), p.52.

25. Hilliard, J.K. and Gries, C.M., 2024. Temporal control of Staphylococcus aureus intracellular pH by sodium and potassium. *FEMS Microbiology Letters*, *371*, p.fnae100.

CHAPTER V

CONCLUDING REMARKS

In this dissertation I conducted research on bacterial communities and populations across different scales of host interactions. Host-pathogen interactions are notoriously difficult to study due to the multifactorial forces that shape these interactions. As a result, research that integrates computational and experimental approaches is desperately needed to generate a more nuanced picture of the forces that shape bacterial colonization and infection of host organisms.

In this thesis, I conducted research on bacteria at both the community and population level. In both efforts I utilized under-appreciated frameworks to add novelty to my work. Chiefly, I invoked theoretical ecological models to better understand the tissue-specific assembly of microbiomes in animals, and later, in Chapter III, leveraged an experimental evolution scheme to understand adaptation of *S. aureus* in the presence of host-encoded stressors. Each of these studies contributed significantly to the fields of microbial ecology and evolution.

In Chapter II, I discovered a link between contributions of neutral processes and the assembly of animal microbiomes in a tissue-specific manner. Importantly, this work represents the first example of a tissue-specific comparison of animal microbiomes across a panel of different hosts. In this chapter, I demonstrate the utility of theoretical ecological models, like the standard neutral community model (SNCM) for identifying broad-scale trends microbiome assembly. Importantly, this work also revealed areas of future research, by highlighting the potentially dynamic nature of microbiomes, stressing the importance of longitudinal sampling designs. Furthermore, this chapter also revealed the importance of carefully considering the source pool of microbes when conducting microbiome studies.

In chapter III I conducted an experimental evolution project to understand how a *S. aureus* adapts to a specific host-encoded pressure. In this project, I serially passaged *S. aureus* populations under increasing concentrations of the polyamine spermine. This work revealed novel connections between potassium transport regulation and antimicrobial resistance, both in response to host-encoded antimicrobials and clinical antibiotics. It also revealed the importance of considering strain-specific diversity, as other each *S. aureus* strain I evolved did garnered mutations in different genes, despite all of them evolving approximately levels of equal spermine resistance.

In chapter IV I hypothesized how mutations I identified in the Ktr potassium transporter may affect the mechanistic function of the transporter, and I provide initial evidence to support these hypotheses. I proposed a set of experiments that will fully elucidate the mechanistic alterations to the Ktr transporter in future studies. I also shared initial findings that provide support for why the populations of *S. aureus* accumulated mutations in the Ktr complex and why this was an evolutionarily successful solution in the context of the selection environment. Extending that, I propose key experiments that will illuminate aspects of Ktr function currently unknown to the field. Specifically, how Ktr-mediated potassium transport may act as a global modulator gene expression in *S. aureus.*

Collectively, this thesis represents a novel set of findings uniquely linking together research in the fields of microbiome science and *S. aureus* biology.

APPENDIX A

SUPPORTING INFORMATION FOR CHAPTER III

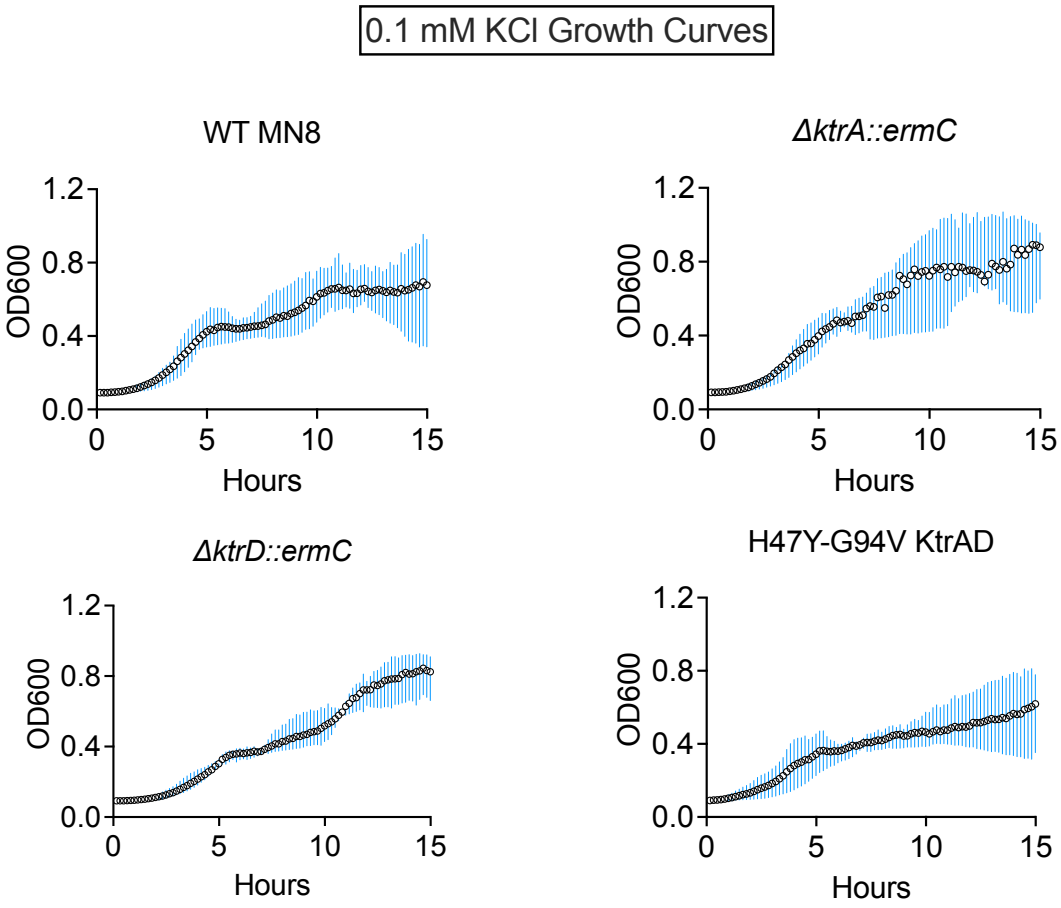

Figure S3.1: Growth curves in defined media with 0.1mM KCl added in. Dots and lines on graphs represent mean and SEM of three independent experiments**.**

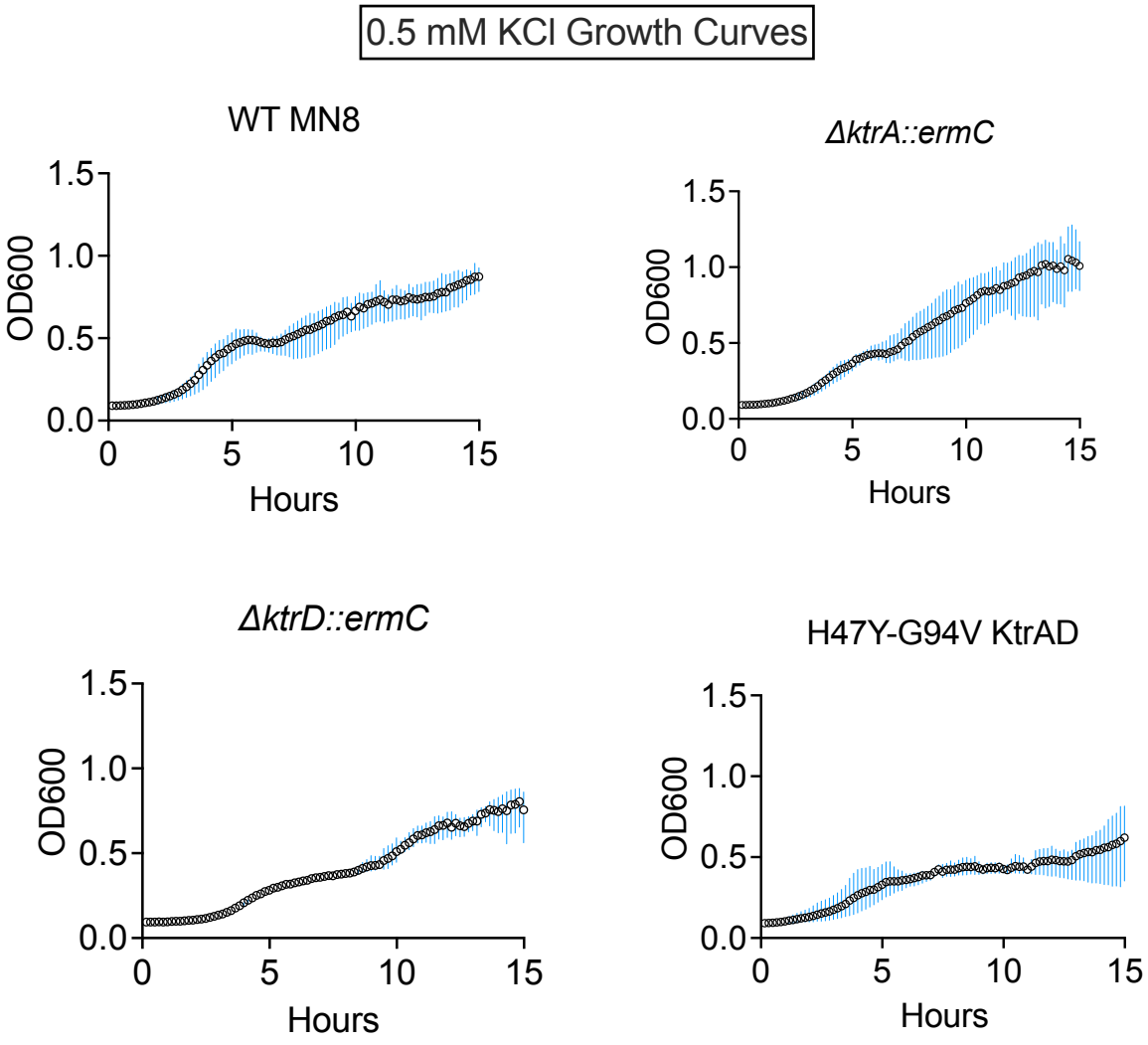

Figure S3.2: Growth curves in defined media with 0.5mM KCl added in. Dots and lines on graphs represent mean and SEM of three independent experiments**.**

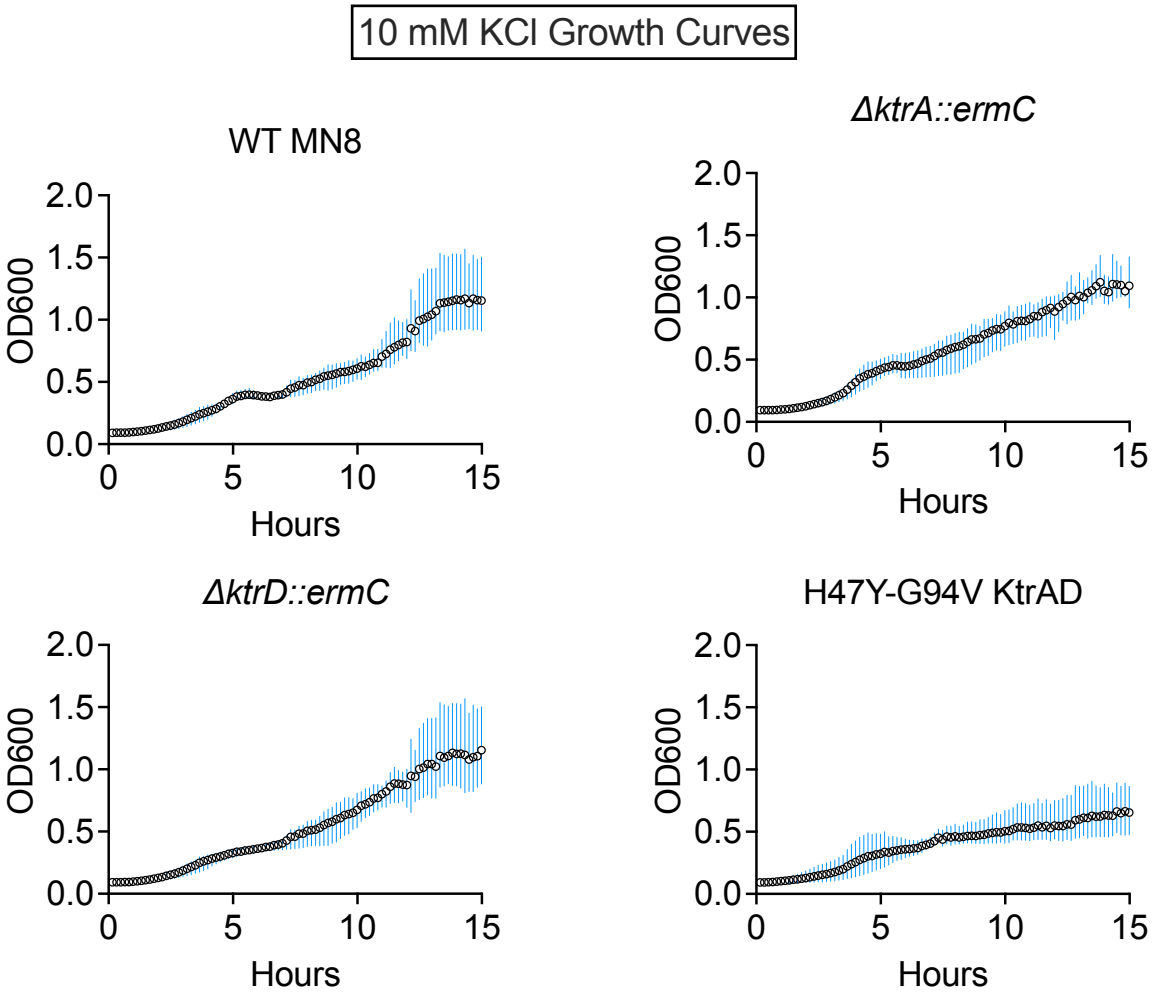

Figure S3.3: Growth curves in defined media with 10 mM KCl added in. Dots and lines on graphs represent mean and SEM of three independent experiments.

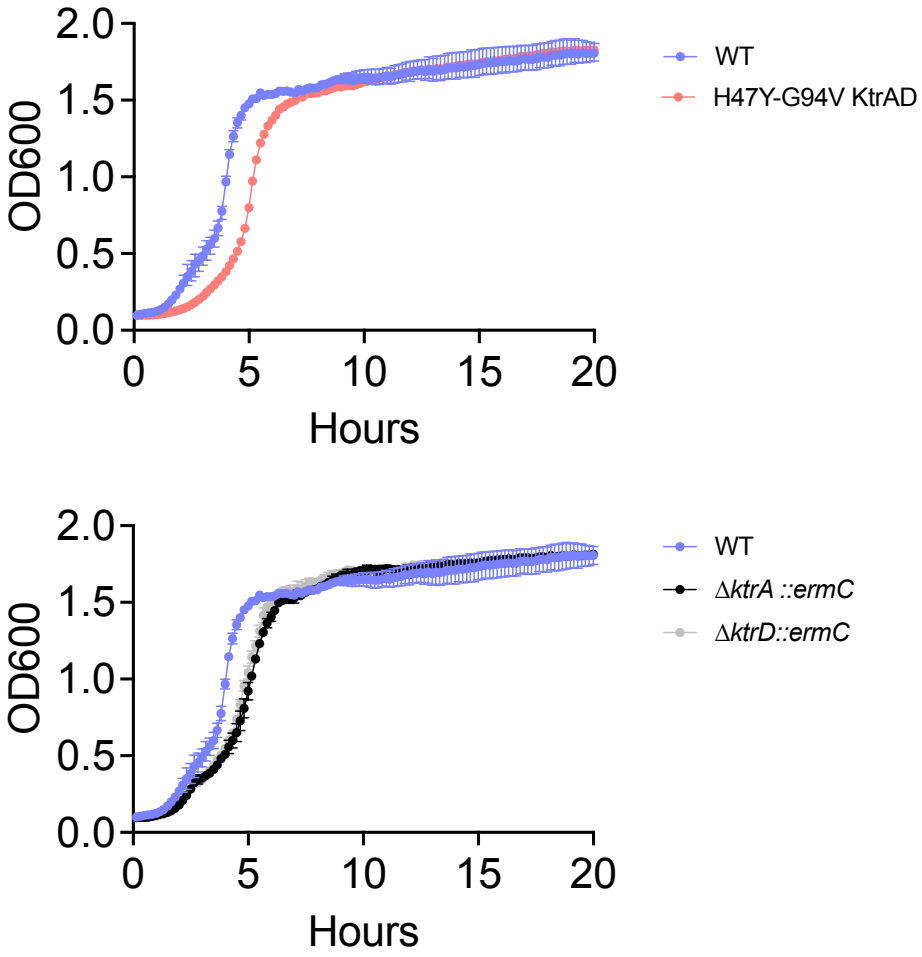

Figure S3.4: Growth curves of different Ktr mutants in TSB.
Graphs represent mean and range of average OD measurements from 3 independent experiments.

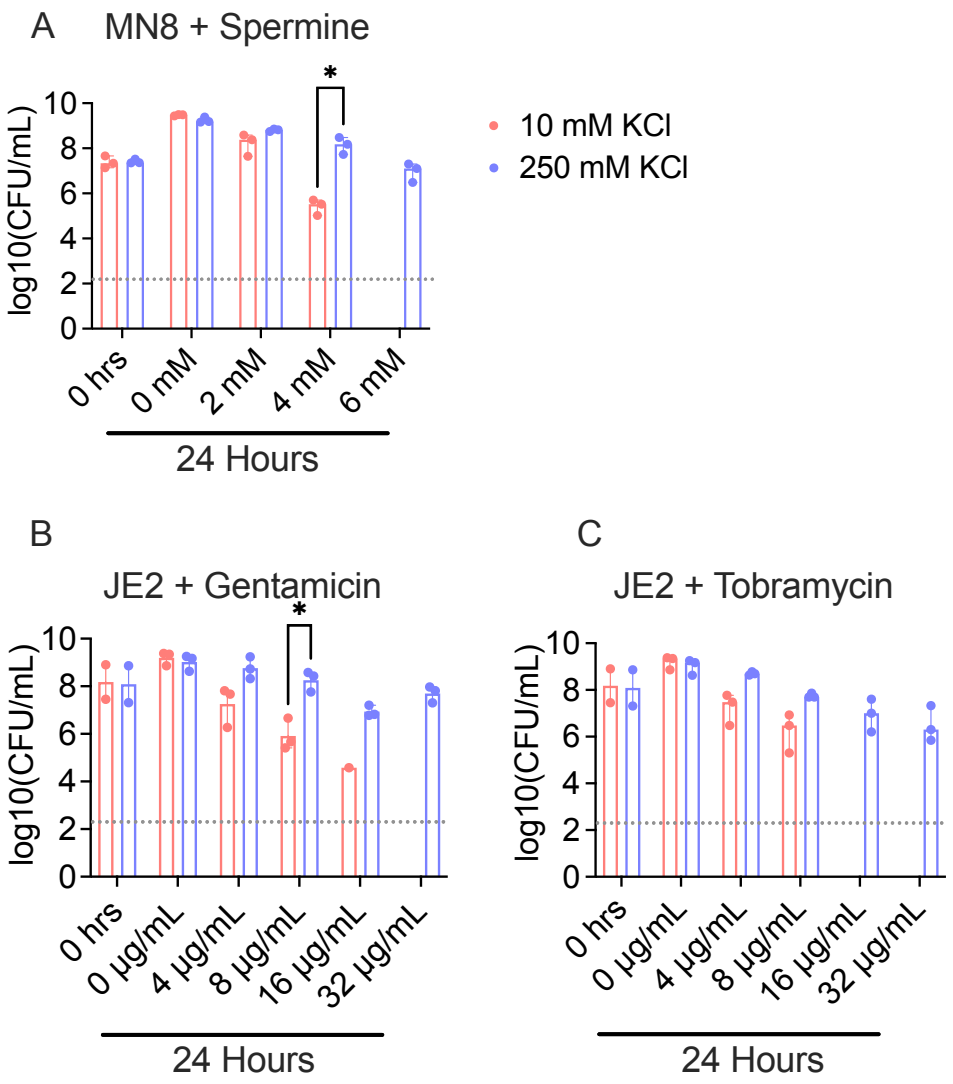

	10 mM KCl	250 mM KCl
Gentamicin	4-8	8-16
Tobramycin	0-2	4-8
Kanamycin	8-16	32-64

Figure S3.5: Effects of supraphysiological potassium concentrations on antimicrobial susceptibility. Enumeration of CFUs after incubation of S. aureus strain MN8 with spermine (A) or S. aureus strain JE2 with aminoglycosides in the presence of exogenous KCl (B,C). Gray dotted line denotes limit of detection. Asterisks denote significant difference in means between two treatments as detected by an unpaired t-test ($P<0.05$). No CFUs were detected for JE2 in 10mM KCl treated with aminoglycosides at concentrations above 8 micrograms/mL. Table (D) depicting MIC values in microgram/mL for different aminoglycoside antibiotics incubated for 24 hours with MN8 in different amounts of KCl.

Table S3.1: Spermine concentrations added at each passage for all spermine-exposed replicates. Spermine concentrations that experimentally evolved populations were exposed to at each passage of the evolution experiment. Spermine was added to the final concentration directly in the growth media.

Passage	Spermine exposure (mM)	Passage saved?
0	0	yes
1	2 mM	no
2	2 mM	no
3	2 mM	no
4	4 mM	yes
5	6 mM	no
6	6 mM	yes
7	6 mM	no
8	6 mM	yes
9	7 mM	no
10	7 mM	yes

Table S3.2: Pilot Evolved Ktr complex Mutations. Mutations that arose in *S. aureus* MN8 *ktrA* and *ktrD* during the pilot evolutionary experiment.

Replicate Line	*ktrA*	*ktrD*
1	H47Y	G94V
2	-	-
3	E76G	M391I
Control	-	-

Table S3.3: List of *S. aureus* strains and their sources used in this study. Single amino acid mutations were introduced into the MN8 parent strain by allelic exchange as outlined in the methods.

Strain	Source	Details
S. aureus MN8	BEI resources	https://www.beiresources.org/Catalog/bacteria/HM-162.aspx
S. aureus HFH-30364	BEI resources	https://beiresources.org/Catalog/bacteria/NR-10189.aspx
S. aureus RN4850	BEI resources	https://www.beiresources.org/Catalog/bacteria/NR-45955.aspx
S. aureus MN8 KtrA:H47Y	This study	Tyrosine substituted for histidine at the 47th position of the KtrA protein in the MN8 strain background
S. aureus MN8 KtrA:G94V	This study	Valine substituted for glycine at the 94thth position of the KtrA protein in the MN8 strain background
S. aureus MN8 KtrA:H47Y-G94V	This study	Tyrosine substituted for histidine at the 47th position of the KtrA protein and valine substituted for glycine at the 94thth position of the KtrA protein in the MN8 strain background
S. aureus MN8 *ktrA::ermC*	This study	*ktrA* gene replaced with erythromycin resistance gene *ermC*
S. aureus MN8 *ktrD::ermC*	This study	*ktrD* gene replaced with erythromycin resistance gene *ermC*

Table S3.4: Ktr complex alleles in published sequencing data. List of mutations in publicly available sequences of *S. aureus* isolates in *ktrA* and *ktrD* genes. Queries were conducted using the identical protein group database on NCBI

Gene	Allele	Strain	Metadata	Sequence ID
ktrA	**A178V**	n/a	clinical or host-associated sample of *S. aureus*	HDB4168921.1
ktrA	A178T	SA-71	n/a	HDB2454818.1
ktrA	**E151V**	CFSA200	clinical or host-associated sample from *S. aureus*	WP_086896505.1
ktrA	E151K	n/a	clinical or host-associated sample from *S. aureus*	HDB5855606.1
ktrA	E76K	SMC9559	Generic sample Host: *Homo sapiens*	WP_217801415.1
ktrA		AF254	clinical or host-associated sample of *S. aureus*	MBV2625534.1
ktrA	**H47Y**	C51	Pig isolate	WP_031790491.1
ktrA		DAR3583	Generic sample Host: *Homo sapiens*	WP_031790491.1
ktrA		RIVM_M084907	Pathogen: clinical or host-associated sample from Staphylococcus aureus	HDE6238165.1
ktrA		RIVM_M085009	Pathogen: clinical or host-associated sample from Staphylococcus aureus	HDE6260146.1
ktrA		RIVM_M043274	Pathogen: clinical or host-associated sample from Staphylococcus aureus	HDF4313963.1
ktrD	**G94V**	H88163	Generic sample Host: *Homo sapiens*	WP_031807927.1
ktrD	G94D	M8158	Pathogen: clinical or host-associated sample from Staphylococcus aureus	HDA5546730.1
ktrD	**Q450K**	CM60	Pathogen: clinical or host-associated sample from Staphylococcus aureus	WP_111088627.1

Table S3.5 All present mutations and their frequencies in passage 10 of the evolution experiment for population MN8-1.

Mutation	Frequency in population	Gene Annotation	Annotated Function
V348L (GTA→CTA)	7.50%	*clpB*	ATP-dependent chaperone protein ClpB
R51T (AGG→ACG)	8.20%	*lipA*	lipoyl synthase
L284I (TTA→ATA)	7.70%	*dnaB*	replicative DNA helicase
V384L (GTA→CTA)	6.10%	*nhaC*	Na+/H+ antiporter family protein
K56* (AAA→TAA)	10.4%	*traE*	Transfer complex protein
E76G (GAA→GGA)	100%	*ktrA*	potassium transport protein regulator
Q450K (CAA→AAA)	26.00%	*ktrD*	potassium transport protein
S135L (TCA→TTA)	61.90%	*ktrD*	potassium transport protein

Table S3.6: All present mutations and their frequencies in passage 10 of the evolution experiment for population MN8-2

Mutation (amino acid)	Frequency in population	Gene Annotation	Annotated Function
V261V (GT**A**→GT**T**)	11.00%	*rpoC*	DNA-directed RNA polymerase, beta' subunit
K283* (**A**AA→**T**AA)	5.30%	*dnaB*	replicative DNA helicase
R114S (AG**A**→AG**T**)	6.70%	*topB*	DNA topoisomerase
Y43C (T**A**C→T**G**C)	39.60%	*apt*	adenine phosphoribosyl transferase
S136P (**T**CT→**C**CT)	100%	hypothetical protein (Pan-genome locus tag: SAUPAN003400000)	predicted: XrtN system VIT domain protein
T366N (A**C**T→A**A**T)	10.80%	*pbp3*	penicillin-binding protein, transpeptidase domain protein
M1K (A**T**G→A**A**G) †	5.70%	*purQ*	phosphoribosylformylglycinamidine synthase I
N86K (AA**T**→AA**A**)		*purS*	phosphoribosylformylglycinamidine synthase, purS protein

Table S3.7: All present mutations and their frequencies in passage 10 of the evolution experiment for population MN8-3.

Mutation	Frequency in population	Gene Annotation	Function
S247C (AGC→TGC)	20.80%	hypothetical protein	DUF536 domain-containing protein
E76G (GAA→GGA)	84.00%	*ktrA*	potassium transport channel regulator
M391I (ATG→ATA)	16.60%	*ktrD*	potassium transport channel
T277N (ACT→AAT)	59.00%	*ktrD*	potassium transport channel

Table S3.8: All present mutations and their frequencies in passage 10 of the evolution experiment for population MN8-4.

Mutation	Frequency in population	Gene Annotation	Function
N28K (AAT→AAA)	6.1%	*ccpA*	catabolite control protein A
L284I (TTA→ATA)	9.3%	*dnaB*	replicative DNA helicase
T278S (ACT→TCT)	8.7%	*dnaB*	replicative DNA helicase
A178V (GCA→GTA)	100.00%	*ktrA*	potassium channel regulator
G94C (GGT→TGT)	100.00%	*ktrD*	potassium transport protein
T277N (ACT→AAT)	59.00%	*ktrD*	potassium transport protein

Table S3.9: All present mutations and their frequencies in passage 10 of the evolution experiment for population HFH-1.

Mutation	Frequency in population	Gene Annotation	Function
G4E (C<u>G</u>A→GAA)	37.1%	*pgl*	6-phosphogluconolactonase
H306Y (<u>C</u>AT→TAT)	60.2%	*pgl*	6-phosphogluconolactonase
P95L (C<u>C</u>G→C<u>T</u>G)	56.8%	*atpA*	atp synthase alpha subunit
M656L (A<u>T</u>G→<u>T</u>TG)	8.1%	*purK*	N5-carboxyaminoimidazole ribonucleotide synthase

Table S3.10: All present mutations and their frequencies in passage 10 of the evolution experiment for population HFH-3.

Mutation	Frequency in population	Gene Annotation	Function
D222Y (GAC→TAC)	7.1%	*mprF*	Phosphatidylglycerol lysyltransferase
G287V (GGT→GTT)	75.3%	*pgl*	6-phosphogluconolactonase
G323D (GGT→GAT	20.9%	*pgl*	6-phosphogluconolactonase

Table S3.11: All present mutations and their frequencies in passage 10 of the evolution experiment for population HFH-4.

\

Mutation	Frequency in population	Gene Annotation	Function
G4E (CGA→GAA)	5.6%	*pgl*	6-phosphogluconolactonase
G120S (GGT→AGT)	75.3%	*pgl*	6-phosphogluconolactonase
R318S (AGA→AGC)	91.1%	*pgl*	6-phosphogluconolactonase
G69R (GGC→CGC)	100%	*lipR*	lysR-type transcriptional regulator

Supplemental table 12: All present mutations and their frequencies in passage 10 of the evolution experiment for populations HFH-5 and HFH-6.

Mutation	Frequency in population	Gene Annotation	Function
L142L (TTA→CTA)	19.7 %	*arcC*	carbamate kinase
Q99* (CAG→TAG)	5.4 %	*mhqA*	Putative ring-cleaving dioxygenase MhqA
C217F (TGT→TTT)	5.1%	*mprF*	phosphatidylglycerol lysyltransferase

Table S3.13: All present mutations and their frequencies in passage 10 of the evolution experiment for population RN-1.

Mutations	Frequency in population	Gene Annotation	Function
A245V (GCA→GTA)	82.4 %	*pgl*	6-phosphogluconolactonase
T10P (ACT→CCT)	13.7%	*pgl*	6-phosphogluconolactonase
Q99* (CAG→TAG)	5.4 %	*mhqA*	Putative ring-cleaving dioxygenase MhqA
F114L (TTT→TTA)	100 %	hypothetical protein	predicted: XrtN system VIT domain protein
T150I (ACT→ATT)	100 %	*bsbh2*	bacillithiol biosynthesis deacetylase BshB2
S147T (AGT→ACT)	13.8%	hypothetical, Pan-locus tag: SAUPAN001647000	phi ETA orf 22-like protein
Q312H (CAG→CAC)	12.6%	*fakA*	fatty acid kinase
S111T (AGT→ACT)	12.2%	hypothetical protein	DUF669 domain-containing protein
A31P (GCA→CCA)	6.8%	*ccpA*	catabolite control protein A
A161P (GCC→CCC)	6.3%	dnaD containing protein	DNA replication initiation protein
R577P (CGC→CCC)	6.2%	*priA*	primosomal protein N helicase

Table S3.14: All present mutations and their frequencies in passage 10 of the evolution experiment for population RN-2.

Mutation	Frequency in population	Gene Annotation	Function
P234L(CCT→CTT)	45.7%	*pgl*	6-phosphogluconolactonase
S41F(TCT→TTT)	10.4%	*pgl*	6-phosphogluconolactonase
G261E (GGG→GAG)	100%	*pgl*	6-phosphogluconolactonase
H138Y (CAT→TAT)	9.3%	*pgl*	6-phosphogluconolactonase
F268V (TTT→GTT)	8.1%	*pgl*	6-phosphogluconolactonase
D216H (GAT→CAT)	6.3%	*cobI*	magnesium transport protein
Δ69 bp	8.3%	*atpG*	atp synthase subunit gamma
R84T (AGA→ACA)	10.7%	*nudF*	nudix hydrolase
D100H (GAT→CAT)	9.6%	hypothetical (*S. aureus* Pan-locus tag: SAUPAN001824000)	phiSLT ORF116b-like protein
A86P (GCA→CCA)	9.5%	*gluD*	glutamate dehydrogenase
A159P (GCG→CCG)	9.3%	dnaD containing protein	DNA replication initiation protein
E68Q (GAG→CAG)	6.1%	hypothetical protein (Pan-locus tag: SAUPAN004460000)	pyridine nucleotide-disulfide oxidoreductase

Table S3.15: All present mutations and their frequencies in passage 10 of the evolution experiment for population RN-3.

Mutations	Frequency in population	Gene Annotation	Function
A245V (GCA→GTA)	31.5%	*pgl*	6-phosphglucolactonase
N143D (AAT→GAT)	52.9%	hypothetical protein (Pan-genome locus tag: SAUPAN003400000)	predicted: XrtN system VIT domain protein
H105Y (CAT→TAT)	39.8%	hypothetical protein (Pan-locus tag: SAUPAN006167000)	hypothetical protein
S136P (TCT→CCT)	39.7%	hypothetical protein	predicted: XrtN system VIT domain protein
S163C (TCT→TGT)	9.6%	*bsaA*	glutathione peroxidase
L261* (TTA→TGA)	6.7%	*atpG*	atp synthase subunit gamma
G207A (GGC→GCC)	5.5%	*capE*	capsular polysaccharide synthesis gene 5E
V173L (GTC→CTC	5.3%	*epiE*	lantibiotic ABC transporter

Table S3.16: All present mutations and their frequencies in passage 10 of of the evolution experiment for population RN-4.

Mutations	Frequency in population	Gene Annotation	Function
S136P (TCT→CCT)	39.7%	hypothetical protein (Pan-genome locus tag: SAUPAN003400000)	predicted: XrtN system VIT domain protein
R116C (CGT→TGT)	28.5%	*sucC*	succinyl-CoA synthetase subunit beta
Δ1 bp	100%	*recJ*	single-stranded DNA exonuclease
Δ6 bp	74.5%	*rpoA*	DNA-directed RNA polymerase subunit alpha
Q170*	14.8%	*atpH*	atp synthase subunit delta
L213* (TTA→TAA)	14.5%	*corA*	magnesium transporter
V310L (GTA→CTA)	11.8%	hypothetical protein (Pan-genome locus: SAUPAN001539000)	phage major capsid protein
L242V (CTT→GTT)	10.10%	hypothetical protein (Pan-genome locus: SAUPAN001168000)	unknown function
S33T (AGC→ACC)	100%	hypothetical protein (locus tag: SAOUHSC_01579)	unknown function
W650S (TGG→TCG)	9.4%	hypothetical protein (Pan-genome tag: SAUPAN002859000)	unknown function
S147T (AGT→ACT)	8.7%	hypothetical (*S. aureus* Pan-locus tag: SAUPAN001824000)	phiSLT ORF116b-like protein
S163C (TCT→TGT)	7.9%	*bsaA*	glutathione peroxidase
A223P (GCT→CCT)	7.7%	*mprF*	phosphatidylglycerol lysyltransferase
E1220D (GAG→GAC)	7.3%	*essC*	type VII secretion protein EssC
Q68* (CAA→TAA)	7.2%	*htrA1*	serine protease
Y43C (TAC→TGC)	5.9%	*apt*	adenine phosphoribosyltransferase